HAPS-based Relaying for Integrated Space-Air-Ground Networks with Hybrid FSO/RF Communication : A Performance Analysis

Swaminathan R[†], Shubha Sharma[*], and A.S.Madhukumar[*]
[†]Discipline of Electrical Engineering, Indian Institute of Technology Indore,
[*]School of Computer Science and Engineering Nanyang Technological University, Singapore
Email: swamiramabadran@iiti.ac.in,{shubha002, asmadhukumar}@ntu.edu.sg

***Abstract*—Optical wireless communication (OWC) has garnered significant importance to provide gigabit capacity links owing to its unique features. Free space optics (FSO) communication, which is the term used for OWC in outdoor scenario, is a good candidate to establish ground-to-satellite/satellite-to-ground links. Despite of many advantages, FSO communication in uplink is limited by the adverse effects of beam wander beam scintillation, and pointing errors. Therefore, to counteract the limitations, it is wise to backup FSO links with reliable radio frequency (RF) links. In addition, the complementary characteristics exhibited by FSO and RF links to atmospheric effects have paved the way for hybrid FSO/RF communication. In recent years, a growing interest is also witnessed in the research and development of space-air-ground integrated network (SAGIN). This paper aims to fuse FSO and RF technologies for integrated space-air-ground uplink networks utilizing unmanned aerial vehicle (UAV) such as high altitude platform station (HAPS) as a relay station for achieving better reliability. Thus, we propose single-hop and SAGIN-based dual-hop system models for uplink satellite communication with hybrid FSO/RF links and the performance is investigated using analytical and simulation results. In summary, the results show that hybrid FSO/RF systems perform better than the FSO systems in uplink scenario due to backup RF link.**

***Index Terms*—Diversity gain, Free space optics, high-altitude platform station (HAPS), hybrid FSO/RF, and space-air-ground integrated network (SAGIN), unmanned aerial vehicle (UAV).**

I. Introduction

According to World Disaster Report 2016 [1], earthquakes, floods, and wildfires have happened on numerous occasions from 2006 to 2015. In addition, it has also been reported that more than 40 percent of the total number of disasters occurred in Asia. Therefore, in order to prevent these disasters, it is important for India and other Asian countries to deploy more satellites and increase the monitoring frequency, observation area, and resolution of images obtained from the satellite. This necessitates the need for large communication capacity and reliable communication links in satellite communication (SATCOM) systems [2], which have opened a new chapter for space-air-ground integrated network (SAGIN) [3] and optical-space-based communication [4]. SAGIN is an integration of satellite system, terrestrial system, and aerial networks in order to achieve a large network topology for efficient sharing of global information. Currently, most of the SAGIN links are operating in microwave radio frequency (RF) band. However, RF band has limited capacity and is also costly as most of the frequency bands are licensed. Also, SAGIN demands high date rate connectivity due to the exchange of huge amount of data among space, air, and ground networks. Thus, FSO communication plays a key role in meeting the high data rate requirements.

In recent years, a growing interest has been witnessed in the research and development of establishing free space optics (FSO) links between ground station (GS) and satellite, which can offer much larger data rates even up to terabits per second. Therefore, it is high time to consider free space optics (FSO) communication, which has attracted enough attention due to various advantages over RF communication such as cheap installation cost with faster deployment, low power usage, high bandwidth, heavily secured links, etc [5]. FSO refers to a line of sight communication using optical carriers between two fixed points in the outdoor environment. Advancement of space technology together with the sophisticated optical sources [6], [7] and detectors opened a new chapter for FSO-based SATCOM. However, the performance of FSO SATCOM links is mainly affected by beam scintillation, beam wander, and pointing errors, which result in frequent link failures [8] and [9]. Beam scintillation and beam wander are atmospheric turbulence effects, which arise due to large-scale inhomogeneities in the turbulent atmosphere. Beam wander is caused by misalignment of the optical beam from the boresight because of the presence of turbulent eddies larger than the beam diameter. Beam scintillation and beam wander lead to loss of signal-to-noise ratio (SNR) at the receiver. In addition, pointing errors, which arises due to misalignment between transmit and receive apertures because of satellite mechanical vibration, is also a primary concern for FSO communication. One efficient solution is to use RF link as a backup with FSO link, as it is less affected by the aforementioned factors. This complementary behaviour of FSO and RF links to atmospheric effects has paved the way for hybrid FSO/RF communication [10].

Another option is to use the concept of relaying technique to counteract atmospheric effects to achieve further improvement in the system performance [11]-[13]. Consequently, SATCOM system during uplink and downlink require a distributed architecture, where data is relayed from GS to relay and then

finally forwarded to the satellite. Unmanned-aerial-vehicles (UAVs) such as high-altitude platform station (HAPS), low-altitude platform station (LAPS), etc. can act as a relay station between GS and satellite to enhance the performance of FSO communication [4]. UAVs should be deployed well above the clouds in such a way that the atmospheric effects on an optical beam is less severe so that a strong line-of-sight (LOS) link exists between UAV and satellite. HAPS is an aerial vehicle usually placed in the stratosphere between 17 and 32 km above sea level [15], where the existence of strong LOS link is possible between HAPS and satellite, which eventually improves the reliability of GS-to-satellite communication link. The main advantages of HAPS are easier and faster deployment than satellite, medium operational costs, easy maintenance, and environmental friendliness. HAPS is useful for many applications such as astronomy, disaster monitoring, ad-hoc communication during disaster situations [16].

By deploying HAPS as a relay terminal, the GS-to-satellite uplink is split into two parts: (i) GS-to-HAPS and (ii) HAPS-to-satellite. Among the two links, GS-to-HAPS link is more sensitive to atmospheric effects. Hence, it is mandatory to backup GS-to-HAPS FSO links with RF links to enhance the link performance. It is also to be noted that HAPS will be located in a cloud-free atmospheric altitude and reliability is not a major concern for HAPS-to-satellite link. Therefore, we can restrict the links to FSO communication alone as shown in Fig. 1(b).

A. Prior Works

In prior works [10] and [17], performance of a terrestrial switching-based single-hop hybrid FSO/RF system was investigated over weak and strong atmospheric turbulence conditions considering log-normal and Gamma-Gamma fading channels, respectively. In both works, the performance analysis was carried out without considering the effect of pointing errors. Further, dual-hop relay-assisted FSO and hybrid FSO/RF communication were investigated extensively for terrestrial communication scenario in [11]-[14]. In [11], end-to-end performance of a dual-hop FSO communication was investigated over Gamma-Gamma turbulence for a fixed gain relaying system. To validate the analytical performance of the dual-hop FSO system, a real state-of-the-art optical hardware system was designed in [12]. In [13], the performance of a switching-based hybrid FSO/RF decode-and-forward (DF) relaying system was investigated considering maximal-ratio-combining (MRC) at the destination. In [14], we considered a dual-hop relaying scenario and optimization of FSO link parameters was carried out for a hybrid FSO/RF system to minimize the effect of pointing errors.

In [18], performance analysis of a hybrid satellite-terrestrial FSO cooperative system had been carried out using satellite RF link, which is modelled using Shadowed-Rician distribution, and terrestrial FSO link, which is modelled using Gamma-Gamma distribution. Similarly, in [19], an integrated satellite-terrestrial relay network considering multiuser environment and threshold-based DF relaying was proposed. Here, the satellite-to-relay link is modelled using Shadowed-Rician distribution and the relay-to-user link is modelled using Nakagami-m distribution. Thus, the proposed works in [18] and [19] investigate the performance of a hybrid satellite-terrestrial relay system, where the ground station receives the signal from the satellite and relay the signals to the destination node. It is to be noted that the ground station acts as a relay node in [18] and [19] and FSO link was used as a last-mile connection from relay to destination node in [18].

In literature, only very few works are reported in case of single-hop FSO communication between satellite and GS [9], [20], and [21]. On contrary, many works are reported considering RF communication between GS and satellite. Recently, in [22], double differential modulation scheme for land mobile satellite (LMS) communication was proposed to overcome the carrier frequency offset and the symbol error probability (SEP) expressions were derived considering shadowed-Rician fading channels. The error performance of the double differential modulation system was compared with coherent modulation and single differential modulation techniques. In addition, the effect of elevation angle on the error performance was also studied. In [9], performance analysis of FSO-based downlink SATCOM system with spatial diversity was carried out over Gamma-Gamma fading channels by deriving closed-form expression for outage probability. In [20], the bit error rate (BER) analysis was carried out for different modulation schemes considering uplink SATCOM system in the presence of atmospheric turbulence and beam-wander induced pointing errors. The atmospheric turbulence was modelled using Gamma-Gamma distribution and the effect of channel anomalies on the BER performance of different intensity modulation schemes was reported. In [21], BER evaluation of various modulation schemes was performed for single-hop FSO-based uplink and downlink SATCOM systems. In addition, aperture averaging scheme was considered to enhance the performance of downlink SATCOM system. In summary, the performance analysis of single-hop RF-based and FSO-based SATCOM systems was investigated in [9], [20]-[22] and link reliability techniques were proposed in case of FSO-based SATCOM system for downlink scenario.

In [25], a LAPS-based based relaying system was proposed recently in which two LAPS serve as relay nodes between terrestrial source and destination nodes. In the proposed work, RF transmission was assumed between LAPS and GS and FSO transmission was assumed between two LAPS. Based on the proposed system model, closed-form expression for outage probability was derived. In [26], the performance of a multibeam very high throughput satellite system was carried out in which GS-to-satellite FSO link was modelled using Gamma-Gamma distribution and satellite-to-user RF link was assumed to follow shadowed-Rician distribution. A cooperative satellite-aerial-terrestrial downlink system based on RF communication was considered in [27] with satellite, UAV, and a group of terrestrial receivers serving as source, relay, and destination nodes, respectively. Here, the coverage

probability of relay-to-destination link and outage performance of source-to-relay link was investigated considering shadowed-Rician fading channel. Recently, outage performance analysis of ground-to-HAPS FSO communication was carried out in [28] assuming log-normal and Gamma-Gamma atmospheric turbulence fading channels with pointing errors. Further, performance of a UAV-to-satellite FSO communication system was studied in [29] and the effect of pointing error and atmospheric turbulence on the BER performance was reported using Monte-Carlo simulations. Recently, we investigated the average SEP performance of HAPS-based hybrid FSO/RF communication for downlink scenario in [30] assuming Gamma-Gamma atmospheric turbulence and Rician RF fading channels.

In order to meet the high data rate requirements of SAGIN, a dual-hop FSO-based uplink SATCOM architecture has been proposed. Further, to counteract the FSO channel distortions and improve the network performance between GS and HAPS, RF backup link is utilized, which leads to the development of HAPS-based SAGIN architecture with hybrid FSO/RF communication. The proposed architecture can be effectively applied in lots of fields such as earth observation and mapping, intelligent transportation system, mission critical applications, disaster monitoring and rescue, etc. with better reliability and high data rates compared to already existing FSO-based SATCOM architecture. In addition, the proposed architecture would bring lots of benefits for 5G and 6G wireless communication systems especially for Enhanced mobile broadband (eMBB), Big communications (BigCom), Ultra- reliable low-latency communications (URLLC), and Three-Dimensional Integrated Communications (3D-InteCom) usage scenarios.

B. Motivations

Thus, the main motivations of our proposed work are as follows:

- The performance analysis of hybrid FSO/RF communication was restricted mostly to terrestrial communication in literature.
- In case of SATCOM systems, the performance analysis was carried out by assuming only FSO link between GS and satellite.
- The FSO link reliability during uplink scenario needs to be improved, as the link is prone to atmospheric turbulence effects, pointing errors, and atmospheric attenuation due to various weather conditions. Moreover, previously proposed aperture averaging scheme also failed to improve the link performance for uplink case.
- In prior works, performance of UAV-to-satellite and ground-to-HAPS FSO communication systems was investigated separately. Further, a comprehensive end-to-end performance analysis based on outage and average SEP was also missing in the existing works.
- Also, UAVs were used as relay nodes only between two terrestrial nodes in most of the existing works. In addition, only RF communication was considered for dual-hop UAV-based relaying system for SATCOM.

TABLE I
RESEARCH STATUS

Type of Communication	**Configuration**	
	Single Hop	**Relay-assisted**
FSO Terrestrial Communication	Well Investigated [8]	Well Investigated [11], [12]
FSO SATCOM	Well Investigated [9], [20], [21], [26]	Moderately Investigated [28], [29]
Satellite-Terrestrial Relay Communication	Not applicable	Well Investigated [18], [19]
Hybrid FSO/RF Terrestrial Communication	Well Investigated [10], [17]	Moderately Investigated [13]
Hybrid FSO/RF SATCOM	Recently we have investigated [30]	Recently we have investigated [30]

- In our work [30], FSO-based dual-hop relaying SATCOM system using HAPS and RF backup links to support FSO links for nullifying atmospheric turbulence effects was proposed. However, the analysis was restricted to downlink scenario without considering the effect of pointing errors and atmospheric attenuation. Further, closed-form expression for average SEP was obtained only for non-coherent detection technique assuming Rician fading for RF communication. Also, asymptotic analysis to obtain full diversity gain from both FSO and RF links was not carried out.

In a nutshell, the overall status of the research works has been tabulated in Table I.

C. Contributions

The major contributions of our work are as follows:

- In our current work, single-hop and SAGIN-based dual-hop system models considering HAPS as a relay station with hybrid FSO/RF communication have been proposed for uplink scenario to counteract the limitations of FSO communication. The system performance of SAGIN-based dual-hop system is studied using single-hop FSO and hybrid FSO/RF systems as benchmark.
- End-to-end average SEP and outage analyses of the hybrid systems have been carried out over Gamma-Gamma distribution in the presence of atmospheric turbulence, attenuation, and pointing errors for FSO communication and Shadowed-Rician distribution for RF communication.
- Unified average SEP and asymptotic SEP expressions are derived in closed-form assuming both intensity modulation and direct detection (IM/DD) and heterodyne detection techniques.
- Asymptotic analysis to obtain full diversity gain from both FSO and RF links has been carried out and the coding and diversity gains obtained due to the presence of RF link has been reported for various scenarios.

The effect of beam-wander induced pointing errors is negligible in case of downlink signals from satellite, as the beam size when reaches the atmosphere is much larger than the turbulent eddy size. However, if the turbulent eddy size is larger than the transmitter beam size, then the effect of beam

wander, which induces pointing error, should be taken into consideration. Thus, beam-wander induced pointing errors has been taken into consideration inside large scale scattering parameter in case of uplink SATCOM scenario.

D. Organization of the manuscript

The manuscript is organized as follows. In Section II, system and channel models have been discussed. The performance analysis of the proposed system models, which include outage, average SEP, and diversity order analyses, is given in Section III. In Section IV, numerical results and related discussions are given for various scenarios. Finally, concluding remarks are given in Section V.

II. System and Channel Models

A. System Model

In our proposed work, we consider two system models. Firstly, we consider a single-hop communication scenario between GS and LEO satellite as shown in Fig. 1(a). Secondly, we consider SAGIN comprising of a GS, a HAPS-based relay node, and a LEO satellite as shown in Fig. 1(b). In case of single-hop communication, we consider both FSO and RF links between GS and satellite with higher priority to FSO link. For SAGIN-based dual-hop communication, both FSO and RF transmission between HAPS and GS and only FSO transmission between satellite and HAPS have been considered. An erroneous DF-relaying-based SATCOM system is assumed in our work. The reason for considering DF relaying is that in case of amplify-and-forward (AF) relaying, the relay node amplifies the received message signal and then forwards the amplified version to the destination node. However, the noise together with the signal is also amplified, which is the main disadvantage of AF relaying scheme. While a conventional DF scheme can completely eliminate noise at the relay, if the relay can make perfect detection. Further, the performance analysis framework in our work is focused on the DF relaying owing to the ease of implementation [23] and the popularity of the DF scheme among the researchers and developers of proof of concept. It is to be noted that in UL scenario, GS and LEO satellite will act as a source (S) node and a destination (D) node, respectively. Further, HAPS will act as a relay (R) node.

The atmospheric channel state in case of FSO communication and flat fading RF channel gain over source-to-destination link are denoted as I_{SD} and h_{SD}, respectively. Moreover, the channel state over source-to-relay and relay-to-destination FSO links are denoted as I_{SR} and I_{RD}, respectively. Similarly, the flat fading RF channel gain over source-to-relay link is denoted as h_{SR}. The system model in case of single-hop communication is straightforward, where source (i.e. GS) transmits to destination (i.e. Satellite), respectively, over FSO or RF links based on the channel conditions. The proposed system model in case of dual-hop communication adopts two-phase orthogonal transmission, where source (i.e. GS) transmits to relay (i.e. HAPS) over FSO or RF link based on the channel conditions during the first phase. After that relay decodes, re-encodes, and forwards the message signal to destination (i.e. LEO satellite) during second phase.

We consider an FSO subsystem with sub-carrier intensity modulation based M-ary phase-shift-keying (SIM-MPSK) at the transmitter. Further, both direct detection and heterodyne detection techniques are assumed at the destination in case of FSO sub-system. In optical SIM-PSK system, the data sequence is first modulated using an electrical modulator considering MPSK scheme, which can be easily implemented with existing microchips. The MPSK signal is then up-converted to an intermediate frequency and the up-converted signal modulates the intensity of the laser beam. At the transmitter of the RF subsystem, the data sequence is modulated using MPSK signalling scheme. The hardware implementation of the hybrid system will also be easier in case of usage of same modulation scheme for both RF and FSO subsystems in electrical domain. It is to be noted that direct detection, which is a non-coherent detection technique, is assumed as the main mode of detection in FSO subsystem. However, heterodyne detection, which is a coherent detection technique, have also been proposed as an alternative detection scheme.

The switching scheme for both single-hop and dual-hop scenarios is described as follows: If the instantaneous signal-to-noise ratio (SNR) of FSO link at the receiver is above a particular FSO threshold SNR value γ_t^f, then FSO link will be used for transmission. However, if the instantaneous SNR drops below γ_t^f, then the receiver sends a 1-bit feedback signal to activate the RF sub-system and the information signal will be transmitted over RF link. Meanwhile, the FSO sub-system will be put on a standby mode. Note that the transmitter does not need the exact channel state information (CSI) of FSO link. As the FSO channel varies on the order of millions of symbol intervals [24], it is not required to monitor the SNR of FSO link at regular intervals unlike RF system to send the feedback signal.

In SATCOM-based FSO communication, the optical beam when propagating through the atmosphere will encounter various kinds of atmospheric effects and they are given as follows [4], [8]: (a) free-space loss (b) atmospheric turbulence effects (c) pointing errors (d) attenuation due to weather conditions. All the above-mentioned effects are taken into consideration in our system model.

The complex baseband signal received at the destination node from source node over single-hop FSO link during uplink transmission is given by

$$y_{SD}^f = \left(\eta_{SD} \, \frac{P_g^f \, G_{Tg}^f \, G_{Rs}^f}{F_L} \, I_{SD} \right)^{b/2} s + n_{SD}^f \,, \qquad (1)$$

where F_L denotes the free-space loss and is given by $F_L = \frac{4\pi L}{\lambda}$, L denotes the transmission distance between GS and satellite, $b = 1$ and 2 for heterodyne and direct detection schemes, respectively, f indicates the transmission over FSO link, η_{SD} denotes the optical-to-electrical conversion coefficient, P_g^f indicates the transmit power of FSO at GS, G_{Tg}^f denotes the transmit telescope gain at GS, G_{Rs}^f denotes the

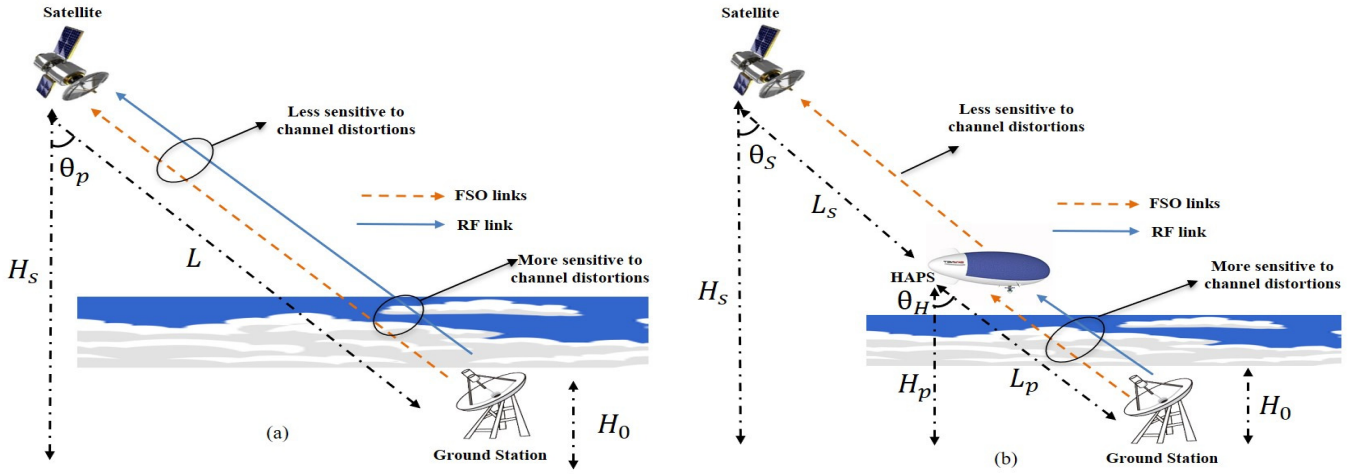

Fig. 1. (a) Single-hop hybrid FSO/RF SATCOM (b) Dual-hop SAGIN

receive telescope gain at LEO satellite, n^f_{SD} denotes the additive white Gaussian noise (AWGN) at the destination, which is a widely accepted model for optical wireless system [8], and symbol s belongs to the MPSK constellation. It is to be noted that $I_{SD} = I^l_{SD} I^a_{SD} I^p_{SD}$ is the product of atmospheric transmittance or atmospheric attenuation due to varying weather conditions I^l_{SD}, atmospheric turbulence I^a_{SD}, and pointing errors I^p_{SD}.

For dual-hop scenario, the complex baseband signal received at the relay node from the source node over FSO link is given by

$$y^f_{SR} = \left(\eta_{SR} \frac{P^f_g \, G^f_{Tg} \, G^f_{Rh}}{F_p} \, I_{SR} \right)^{b/2} s + n^f_{SR} \,, \tag{2}$$

where the free space loss F_p is given by $F_p = \frac{4\pi L_p}{\lambda}$, L_p denotes the transmission distance between GS and HAPS, $I_{SR} = I^l_{SR} I^a_{SR} I^p_{SR}$, n^f_{SR} denotes the AWGN at the relay during FSO transmission, and G^f_{Rh} denotes the receive telescope gain at LEO satellite. After decoding the information signal at the relay, the decoded symbol $\hat{s}$ will be forwarded to the destination and the received complex baseband signal at the destination over FSO link is given by

$$y^f_{RD} = \left(\eta_{RD} \frac{P^f_h \, G^f_{Th} \, G^f_{Rs}}{F_s} \, I_{RD} \right)^{b/2} \hat{s} + n^f_{RD} \,, \tag{3}$$

where $I_{RD} = I^a_{RD} I^p_{RD}$, free-space loss F_s is given by $F_s = \frac{4\pi L_s}{\lambda}$, L_s denotes the transmission distance between HAPS and satellite, λ denotes the wavelength of FSO signal, and n^f_{RD} denotes the AWGN at the destination during FSO transmission. Since HAPS will be usually deployed in a cloud-free atmospheric altitude, the atmospheric attenuation due to varying weather condition I^l_{RD} will be almost equal to unity and hence, the same has been ignored in (3).

In case of single-hop scenario, the received complex baseband signal at the destination over RF link is given by

$$y^r_{SD} = h_{SD} \sqrt{P^r_g \, g^r_{SD}} \, s + n^r_{SD} \,, \tag{4}$$

where r indicates the transmission over RF link, P^r_g indicates the transmit RF power at GS, g^r_{SD} is the pathloss of RF link from GS to satellite, and n^r_{SD} denotes the AWGN at the destination during RF transmission.

In case of dual-hop transmission, the received complex baseband signal at the relay over RF link is given by

$$y^r_{SR} = h_{SR} \sqrt{P^r_g \, g^r_{SR}} \, s + n^r_{SR} \,, \tag{5}$$

where g^r_{SR} is the pathloss of RF link from GS to HAPS and n^r_{SR} denotes the AWGN at the relay node during RF transmission.

From the received complex baseband signals, the instantaneous SNR expression [33] for source-to-destination and source-to-relay FSO links assuming both hetrodyne and direct detection schemes are, respectively, given by

$$\gamma^f_{SD} = \frac{(\eta_{SD} \, P^f_g \, G^f_{Tg} \, G^f_{Rs} \, I_{SD})^b}{(F_L)^b (\sigma^f_{SD})^2} \,, \tag{6}$$

$$\gamma^f_{SR} = \frac{(\eta_{SR} \, P^f_g \, G^f_{Tg} \, G^f_{Rh} \, I_{SR})^b}{(F_p)^b (\sigma^f_{SR})^2} \,, \tag{7}$$

The instantaneous SNR expression for relay-to-destination FSO link is given by

$$\gamma^f_{RD} = \frac{(\eta_{RD} \, P^f_h \, G^f_{Th} \, G^f_{Rs} \, I_{RD})^b}{(F_s)^b \, (\sigma^f_{RD})^2} \,, \tag{8}$$

where $(\sigma^f_{ii})^2$ denotes the noise variance of AWGN channel over FSO link. Now the corresponding average SNR expressions [33] are given by

$$\Gamma^f_{SD} = \frac{(\eta_{SD} \, P^f_g \, G^f_{Tg} \, G^f_{Rs} \, k_{SD} \, I^l_{SD} \, A_0)^b}{(F_L)^b \, (\sigma^f_{SD})^2} \,, \tag{9}$$

$$\Gamma^f_{SR} = \frac{(\eta_{SR} \, P^f_g \, G^f_{Tg} \, G^f_{Rh} \, k_{SR} I^l_{SR} \, A_0)^b}{(F_p)^b \, (\sigma^f_{SR})^2} \,, \tag{10}$$

$$\Gamma^f_{RD} = \frac{(\eta_{RD} \, P^f_h \, G^f_{Th} \, G^f_{Rs} \, k_{RD} \, A_0)^b}{(F_s)^b \, (\sigma^f_{RD})^2} \,, \tag{11}$$

where A_0 is the fraction of total power collected at the receiver aperture, ζ_{ii} is the pointing errors parameter or coefficient, and $k_{ii} = \frac{\zeta_{ii}^2}{\zeta_{ii}^2+1}$.

Similarly, the instantaneous and average SNR expressions for RF link from the baseband signal are, respectively, given by

$$\gamma_{jj}^r = \frac{P_g^r \, g_{jj}^r \, |h_{jj}|^2}{(\sigma_{jj}^r)^2} \quad , \Gamma_{jj}^r = \frac{P_g^r \, g_{jj}^r \, \Omega_{jj}}{(\sigma_{jj}^r)^2} \, , \tag{12}$$

where $jj \in \{SD, SR\}$, $(\sigma_{ii}^r)^2$ denotes the noise variance of AWGN channel over RF link, $\Omega_{jj} = \mathbb{E}[|h_{jj}|^2]$ indicates the average power of line-of-sight (LOS) and non-line-of-sight (NLOS) or scattered components, and $\mathbb{E}[\cdot]$ denotes the expectation operator. The noise variance is given by $(\sigma_{jj}^r)^2 = P_N N_F$, N_F denotes the noise figure of the receiver, $P_N(\text{dB}) = K_{\text{dB}} + T_N + \text{BW}$, BW denotes the receiver noise bandwidth (in dBHz), T_N indicates the system noise temperature (in dBK), and K_{dB} is the Boltzmann's constant, which is equal to -228.6 dBW/K/Hz. The pathloss of RF link g_{jj}^r is given by [31], [32]

$$g_{jj}^r[dB] = G_T + G_R - L_F - L_R - L_A - L_O \, , \tag{13}$$

where G_T indicates the transmit antenna gain (in dB), G_R indicates the receive antenna gain (in dB), L_F denotes the free space loss (in dB) and is given by $L_F = 92.45 + 20 \log f + 20 \log L_p$ for source-to-relay link (GS-to-HAPS) scenario, $L_F = 20\log\left(\frac{4\pi L}{\lambda_r}\right)$ for source-to-destination (GS-to-Satellite), λ_r denotes the wavelength of RF signal, f denotes the RF frequency in GHz, L denotes the transmission distance between GS and satellite (in m), L_p denotes the transmission distance between GS and HAPS (in Km), L_R denotes the rain attenuation in dB/Km, L_A denotes the gaseous atmosphere loss, and L_O denotes the other fading or miscellaneous losses (in dB) that include antenna mispointing, polarization mismatch, antenna degradation, etc.

B. Channel Models

FSO channel: The atmospheric turbulence-induced fading or the fluctuations in received optical irradiance I_{ii}^a is modeled using Gamma-Gamma distribution, which is used to characterize moderate to strong atmospheric turbulence condition. We have used Gamma-Gamma distribution due to its wide acceptance in the current literature [5], [9], [11], [13], [18], [20], [21]. It is a doubly-stochastic scintillation model, where the received optical irradiance I_{ii}^a is considered as a product of two independent Gamma random variables, which represent the intensity fluctuations due to small and large scale turbulence. The PDF of I_{ii}^a is given by [5, eq.(2)]

$$f_{I_{ii}^a}(x) = \frac{2(\alpha_{ii}\beta_{ii})^{\frac{\alpha_{ii}+\beta_{ii}}{2}} x^{\frac{\alpha_{ii}+\beta_{ii}}{2}-1}}{\Gamma(\alpha_{ii})\Gamma(\beta_{ii})} \times K_{\alpha_{ii}-\beta_{ii}}(2\sqrt{\alpha_{ii}\beta_{ii}x}) \, , \;\; x > 0 \tag{14}$$

where $ii \in \{SD, SR, RD\}$, α_{ii} and β_{ii} are the large scale and small scale turbulence parameters of the scattering environment, respectively, $K_v(\cdot)$ indicates the modified bessel function of second kind of order v [39, eq.(8.407.1)], and $\Gamma(\cdot)$ is the gamma integral function [39, eq.(8.310.1)]. The expressions to calculate α_{ii} and β_{ii} for SATCOM links are given in Appendix B. The attenuation due to pointing error can be expressed as $I_{ii}^p \approx A_0 \exp\left(-\frac{2r_0^2}{(W_{Leq}^{ii})^2}\right)$, where r_0 indicates the radial displacement between beam center and detector center and is modelled using Rayleigh distribution and W_{Leq}^{ii} is the equivalent beam waist at the receiver [14]. Now the probability density function (PDF) of pointing errors I_{ii}^p is given by [26, Eq.(2)]

$$f_{I_{ii}^p}(y) = \frac{\zeta_{ii}^2}{A_0^{\zeta_{ii}^2}} y^{\zeta_{ii}^2 - 1} \tag{15}$$

The attenuation due to path loss or atmospheric transmittance for source-to-destination and source-to-relay FSO links are determined using Beers-Lambert law [4], [40] and are given by $I_{SD}^l = \exp\left(-\int_0^L \sigma(z).dz\right)$ and $I_{SR}^l = \exp\left(-\int_0^{L_p} \sigma(z).dz\right)$, respectively, and $\sigma(z)$ is the atmospheric attenuation coefficient which depends on the propagation distance. It is to be noted that MODTRAN 4.0 simulations [40] will give the measure of atmospheric transmittance. The combined PDF of atmospheric channel state of FSO link $I_{ii} = I_{ii}^l I_{ii}^a I_{ii}^p$ can be written in terms of Meijer G-function $G_{p,q}^{m,n}(\cdot)$ using [34, Eq.(07.34.03.0605.01)] (i.e. using (48) in Appendix A) and is given by [33, Eq.(1)]

$$f_{I_{ii}}(I) = \frac{\zeta_{ii}^2}{I\Gamma(\alpha_{ii})\Gamma(\beta_{ii})} G_{1\;3}^{3\;0}\left(\frac{\alpha_{ii}\beta_{ii}I}{A_0}\middle| \begin{matrix}\zeta_{ii}^2+1 \\ \zeta_{ii}^2, \alpha_{ii}, \beta_{ii}\end{matrix}\right) \tag{16}$$

The PDF of the instantaneous SNR of FSO links can be obtained from (16) using the power transformation of random variable and the resultant unified PDF expression is given by [33, Eq.(4)]

$$f_{\gamma_{ii}^f}(\gamma_{ii}) = \frac{\mathcal{A}_{ii}}{\gamma_{ii}} G_{1\;3}^{3\;0}\left(D_{ii}\left(\frac{\gamma_{ii}}{\Gamma_{ii}^f}\right)^{1/b}\middle| \begin{matrix}\zeta_{ii}^2+1 \\ \zeta_{ii}^2, \alpha_{ii}, \beta_{ii}\end{matrix}\right) \, , \tag{17}$$

where $\mathcal{A}_{ii} = \frac{\zeta_{ii}^2}{b\Gamma(\alpha_{ii})\Gamma(\beta_{ii})}$ and $D_{ii} = \alpha_{ii}\beta_{ii}k_{ii}$. The cumulative distribution function (CDF) of γ_{ii}^f using [34, Eq.(07.34.21.0084.01)] is given by

$$F_{\gamma_{ii}^f}(\gamma_{ii}) = \mathcal{F}_{ii} G_{b+1\;\;3b+1}^{3b\;\;\;1}\left(\frac{D_{ii}^b \gamma_{ii}}{b^{2b}\Gamma_{ii}^f}\middle| \begin{matrix}1, \mathcal{E}_{ii}^1 \\ \mathcal{E}_{ii}^2, 0\end{matrix}\right) \, , \tag{18}$$

where $\mathcal{F}_{ii} = \frac{\zeta_{ii}^2 b^{\alpha_{ii}+\beta_{ii}-2}}{(2\pi)^{b-1}\Gamma(\alpha_{ii})\Gamma(\beta_{ii})}$, $\mathcal{E}_{ii}^1 = \left\{\frac{\zeta_{ii}^2+1}{b}, \ldots, \frac{\zeta_{ii}^2+b}{b}\right\}$, and $\mathcal{E}_{ii}^2 = \left\{\frac{\zeta_{ii}^2}{b}, \ldots, \frac{\zeta_{ii}^2+b-1}{b}, \frac{\alpha_{ii}}{b}, \ldots, \frac{\alpha_{ii}+b-1}{b}, \frac{\beta_{ii}}{b}, \ldots, \frac{\beta_{ii}+b-1}{b}\right\}$,

RF channel: In our work, we consider Shadowed-Rician distribution, which fits very well for modelling satellite communication links [36]. It is a generalized RF fading channel model which includes Rayleigh and Rician distribution as special cases [37], [38]. In case of Shadowed-Rician fading model, the amplitude of the LOS component is assumed to be random unlike Rician model and it finds potential applications in different frequency bands such as the UHF band, C-band, L-band, S-band, C-band, and Ka-band [36].

The lowpass-equivalent complex envelope of the Shadowed-Rician fading channel model can be written as follows [36]: $h_{ii}(t) = A(t)\text{exp}(j\alpha(t))+Z(t)\text{exp}(j\zeta_0)$, where $j^2=-1$, $\alpha(t)$ is the stationary random phase process which follows uniform distribution over $[0, 2\pi)$, and ζ_0 indicates the deterministic phase of the LOS component. Note that the stationary independent random processes $Z(t)$ and $A(t)$ denote the amplitude of LOS and NLOS components and they follow Rayleigh and Nakagami-m distributions, respectively. Now the Shadowed-Rician PDF of envelope of fading channel gain h_{jj} (i.e. $|h_{jj}|$) is given by [1][35, eq.(2.67)]

$$f_{|h_{jj}|}(h') = \left(\frac{2b_1m_1}{2b_1m_1\Omega_1}\right)^m \frac{h'}{b_1}\text{exp}\left(\frac{-(h')^2}{2b_1}\right) \times {}_1F_1\left(m_1;1;\frac{\Omega_1(h')^2}{2b_1(2b_1m_1+\Omega_1)}\right), \quad (19)$$

${}_1F_1(\cdot;\cdot;\cdot)$ is the confluent hypergeometric function [39], $2b_1$ is the average power of NLOS components, Ω_1 is the average power of LOS component, and $0 \le m_1 \le \infty$ is the Nakagami-m fading severity parameter.

Applying power transformation of random variable in (19) using (12), we obtain the PDF of instantaneous SNR of RF link, which is given by

$$f_{\gamma^r_{jj}}(\gamma'_{jj}) = \frac{\Omega_{jj}\alpha_1}{\Gamma^r_{jj}}\text{exp}\left(-\frac{\beta_1\Omega_{jj}\gamma'_{jj}}{\Gamma^r_{jj}}\right){}_1F_1\left(m_1;1;\frac{\Omega_{jj}\delta_1\gamma'_{jj}}{\Gamma^r_{jj}}\right), \quad (20)$$

where $\Omega_{jj} = \Omega_1 + 2b_1$, $\alpha_1 = \frac{(2b_1m_1/(2b_1m_1+\Omega_1))^{m_1}}{2b_1}$, $\beta_1 = \frac{1}{2b_1}$, and $\delta_1 = \frac{0.5\Omega_1}{2b_1^2m_1+b_1\Omega_1}$. It is to be noted that for $m_1 = 0$ and $m_1 = \infty$, the norm of h_{jj} (i.e. $|h_{jj}|$) follows Rayleigh and Rician distributions, respectively. The CDF of γ^r_{jj} using Kummer transformation [41, eq.(12)] is given by

$$F_{\gamma^r_{jj}}(\gamma'_{jj}) = \sum_{k_1=0}^{m_1-1} \frac{\Omega_{jj}\alpha_1\psi(k_1)}{((\beta_1-\delta_1)\Omega_{jj})^{k_1+1}} \times \gamma\left(k_1+1, \frac{(\beta_1-\delta_1)\gamma'_{jj}\Omega_{jj}}{\Gamma^r_{jj}}\right), \quad (21)$$

where $\psi(k_1) = \frac{(m_1-1)!\delta_1^{k_1}(\Omega_1)^{k_1}}{(m_1-1-k_1)!\,(k_1!)^2}$ and $\gamma(\cdot,\cdot)$ represents lower incomplete gamma function [39].

III. Performance Analysis

In this section, we perform the outage and error analyses of single-hop and dual-hop SATCOM systems and derive the closed-form expressions for outage and average SEP. In addition, asymptotic outage and average SEP expressions are also derived to obtain the diversity gain of the proposed system models.

[1]For simplicity without loss of generality, we are not using the index t in our derivation.

A. Outage analysis of single-hop SATCOM:

The single-hop hybrid FSO/RF-based SATCOM will be in outage, when both FSO and RF links are lesser than their respective threshold values γ^f_t and γ^r_t, respectively. Hence, the outage probability is given by

$$P^{out}_{SD} = F_{\gamma^f_{SD}}(\gamma^f_t)\, F_{\gamma^r_{SD}}(\gamma^r_t), \quad (22)$$

where the CDFs of FSO and RF links are given by (18) and (21), respectively.

B. Outage analysis of dual-hop SATCOM:

The dual-hop SATCOM system with hybrid FSO/RF and FSO links will not be in outage if both the links are above their respective threshold values. So, the probability that the system will be in outage is given by

$$\begin{aligned} P^{out}_{DH} &= 1-\{(1-P^{out}_{SR})(1-P^{out}_{RD})\} \\ &= P^{out}_{SR}+P^{out}_{RD}-P^{out}_{SR}P^{out}_{RD}, \end{aligned} \quad (23)$$

where individual terms are given by $P^{out}_{RD} = F_{\gamma^f_{RD}}(\gamma^f_t)$ and $P^{out}_{SR} = F_{\gamma^f_{SR}}(\gamma^f_t)\, F_{\gamma^r_{SR}}(\gamma^r_t)$

C. Error analysis of single-hop SATCOM:

The conditional SEP of MPSK signaling conditioned on the instantaneous SNR of a given link can be written as [13, eq.(14)]

$$p(e/\gamma_{ii}) = \frac{A}{2}\text{erfc}\left(\sqrt{\gamma_{ii}}B\right), \quad (24)$$

where $A=1$ when modulation order M=2 i.e. binary phase-shift keying (BPSK), $A=2$ when $M>2$, B = $\sin(\pi/M)$, and erfc$(\cdot)$ denotes the complementary error function. Using the relation between erfc$(\cdot)$ and Meijer G-function [34, Eq.(07.34.03.0619.01)] (i.e. using (47) in Appendix A), the conditional SEP can also be written in terms of Meijer G-function and is given by

$$p(e/\gamma_{ii}) = \frac{A}{2\sqrt{\pi}}G^{\,2\,0}_{\,1\,2}\left(B^2\gamma_{ii}\middle|\begin{matrix}1\\0,1/2\end{matrix}\right), \quad (25)$$

The conditional SEP can also be expressed in terms of Maclaurin series expansion [39, eq.(3.321)] and is given by

$$p(e/\gamma_{ii}) = \frac{A}{2}\left\{1-\frac{2}{\sqrt{\pi}}\sum_{k=0}^{\infty}\frac{(-1)^k(\gamma_{ii})^{\frac{2k+1}{2}}B^{2k+1}}{k!(2k+1)}\right\}. \quad (26)$$

The average SEP of single-hop SATCOM considering hybrid FSO/RF links is given by

$$\bar{P}_{eSD} = B^f_{SD}(\gamma^f_t) + F_{\gamma^f_{SD}}(\gamma^f_t)\, B^r_{SD}, \quad (27)$$

where $B^f_{SD}(\gamma^f_t)$ denotes the average SEP of SH FSO link when $\gamma^f_{SD} > \gamma^f_t$, $F_{\gamma^f_{SD}}(\gamma^f_t)$ indicates the outage probability

of FSO link, and B^r_{SD} denotes the average SEP of single-hop RF link. Now $B^f_{SD}(\gamma^f_t)$ can be derived as follows:

$$B^f_{SD}(\gamma^f_t) = \int_{\gamma^f_t}^{\infty} p(e/\gamma^f_{SD}) f_{\gamma^f_{SD}}(\gamma_{SD})\, d\gamma_{SD} \tag{28}$$

$$= \underbrace{\int_0^{\infty} p(e/\gamma^f_{SD}) f_{\gamma^f_{SD}}(\gamma_{SD}) d\gamma_{SD}}_{I_1} - \underbrace{\int_0^{\gamma^f_t} p(e/\gamma^f_{SD}) f_{\gamma^f_{SD}}(\gamma_{SD}) d\gamma_{SD}}_{I_2(\gamma^f_t)} \tag{29}$$

Now (29) is divided into two terms I_1 and $I_2(\gamma^f_t)$. The detailed derivation of I_1 and $I_2(\gamma^f_t)$ is given in Appendix C. The outage probability of FSO subsystem, which is denoted by $F_{\gamma^f_{SD}}(\gamma^f_t)$, considering single-hop scenario can be obtained from (18).

The average SEP of RF link is given by

$$B^r_{SD} = \int_0^{\infty} p(e/\gamma^r_{SD}) f_{\gamma^r_{SD}}(\gamma_{SD}) d\gamma_{SD}\,. \tag{30}$$

After substituting (20) and (24) in (30), ${}_1F_1(\cdot;\cdot;\cdot)$ is expanded in terms of Kummer transformation [41, eq.(12)] and then using integration by parts, the integral in (30) is simplified to obtain the final expression as

$$B^r_{SD} = \frac{A\Omega_{SD}\alpha_1}{2} \sum_{k_1=0}^{m_1-1} \frac{\psi(k_1)}{(\Gamma^r_{SD})^{k_1+1}} \left\{ \frac{\Gamma(k_1+1)}{C^{k_1+1}} - \frac{Bk_1!}{\sqrt{\pi}} \sum_{n=0}^{k_1} \frac{\Gamma(n+0.5)}{n! C^{k_1+1-n}(B^2+C)^{n+0.5}} \right\}, \tag{31}$$

where $C = \frac{(\beta_1-\delta_1)\Omega_{SD}}{\Gamma^r_{SD}}$.

D. Error analysis of dual-hop SATCOM

As per the proposed system model for dual-hop scenario, if the instantaneous SNR of FSO link between source (i.e. GS) and relay (i.e. HAPS) is above a threshold SNR value, then FSO link will be used for transmission. If the instantaneous SNR is less than a threshold value, then RF link will be used for transmission between source and relay. Further, only FSO link will be used between relay and destination (i.e. LEO satellite). Now the average SEP of source-to-relay-to-destination link is obtained by averaging the conditional SEP of source-to-relay-to-destination link over the PDFs of instantaneous SNR of source-to-relay and relay-to-destination links based on the conditions $\gamma^f_{SR} > \gamma_t$ and $\gamma^f_{SR} < \gamma_t$, which is given by (32) (refer to the top of next page), where $P_{eSRD}(\gamma^f_{SR}, \gamma^f_{RD})$ is the conditional SEP of source-to-relay-to-destination link conditioned on γ^f_{SR} and γ^f_{RD}. Further, $P_{eSRD}(\gamma^r_{SR}, \gamma^f_{RD})$ is the conditional SEP of source-to-relay-to-destination link conditioned on γ^r_{SR} and γ^f_{RD}. The conditional SEP of FSO-based source-to-relay and relay-to-destination links assuming $M-$ ary signalling can be written as [42, eq.(21)]

$$P_{eSRD}(\gamma^f_{SR}, \gamma^f_{RD}) = P(e/\gamma^f_{SR}) + P(e/\gamma^f_{RD}) - P(e/\gamma^f_{SR})\ P(e/\gamma^f_{RD})\,. \tag{33}$$

Similarly, the conditional SEP of RF-based source-to-relay and FSO-based relay-to-destination links assuming $M-$ ary signalling can be written as [42, eq.(21)]

$$P_{eSRD}(\gamma^r_{SR}, \gamma^f_{RD}) = P(e/\gamma^r_{SR}) + P(e/\gamma^f_{RD}) - P(e/\gamma^r_{SR})\ P(e/\gamma^f_{RD})\,. \tag{34}$$

After substituting (33) and (34) in (32), the average SEP of dual-hop SATCOM can be written as

$$\bar{P}_{eSRD} = B^f_{SR}(\gamma_t) + F_{\gamma^f_{SR}}(\gamma_t) B^r_{SR} + B^f_{RD} - B^f_{RD}\left\{ B^f_{SR}(\gamma_t) + F_{\gamma^f_{SR}}(\gamma_t) B^r_{SR} \right\}, \tag{35}$$

where B^f_{RD} denotes the average SEP of relay-to-destination FSO link, $B^f_{SR}(\gamma_t)$ indicates the average SEP of source-to-relay FSO link when $\gamma^f_{SR} > \gamma_t$, and B^r_{SR} indicates the average SEP of source-to-relay RF link. From (35), the average SEP can be written as

$$\bar{P}_{eSRD} = \bar{P}_{eSR} + \bar{P}_{eRD} - \bar{P}_{eSR}\ \bar{P}_{eRD}\,, \tag{36}$$

where $\bar{P}_{eRD} = B^f_{RD}$, which is obtained from (57) given in Appendix C by replacing D_{SD}, $\mathcal{F}_{SD}$, and $\mathcal{E}_{SD}$ with D_{RD}, $\mathcal{F}_{RD}$, and $\mathcal{E}_{RD}$, respectively. Note that $\bar{P}_{eSR}$ in (36) is the average SEP of hybrid FSO/RF link, which is given by

$$\bar{P}_{eSR} = B^f_{SR}(\gamma^f_t) + F_{\gamma^f_{SR}}(\gamma^f_t)\, B^r_{SR}\,. \tag{37}$$

$\bar{P}_{eSR}$ can be obtained similar to (27) by replacing D_{SD}, $\mathcal{F}_{SD}$, $\mathcal{C}_{SD}$, $\mathcal{E}_{SD}$, Ω_{SD}, and Γ^r_{SD} with D_{SR}, $\mathcal{F}_{SR}$, $\mathcal{C}_{SR}$, $\mathcal{E}_{SR}$, Ω_{SR}, and Γ^r_{SR}.

E. Asymptotic Analysis

The asymptotic expressions for outage and average SEP have also been derived in closed-form to obtain the diversity gain of SH and DH systems. The asymptotic outage probability expression for the single-hop hybrid FSO/RF SATCOM system when $\Gamma^f_{SD} \to \infty$ is given by

$$P^{aout}_{SD} = F_{\gamma^{asy}_{SD}}(\gamma^f_t)\, F_{\gamma^r_{SD}}(\gamma^r_t)\,. \tag{38}$$

The asymptotic expression for CDF of FSO link in (38) is obtained by applying [34, eq.(07.34.06.0040.01)] on (18) and the same is given by

$$F_{\gamma^{asy}_{ii}}(\gamma^f_t) = \mathcal{F}_{ii} \sum_{l=1}^{3b} \frac{\prod_{\substack{x=1 \\ x\neq l}}^{3b} \Gamma(\mathcal{E}^{2,x}_{ii} - \mathcal{E}^{2,l}_{ii})}{\mathcal{E}^{2,l}_{ii} \prod_{x=1}^{b} \Gamma(\mathcal{E}^{1,x}_{ii} - \mathcal{E}^{2,x}_{ii})} \left(\frac{D_{ii}\gamma^f_t}{b^{2b}\Gamma^f_{ii}} \right)^{\mathcal{E}^{2,l}_{ii}}, \tag{39}$$

where $\mathcal{E}^{i,x}_{ii}$ represents the x^{th} term of $\mathcal{E}^i_{ii}$. From (38) and (39), it is observed that $P^{aout}_{SD} \propto (\Gamma^f_{SD})^{-v_{SD}}$, where $v_{SD} = \min\left(\frac{\zeta^2_{SD}}{b}, \frac{\alpha_{SD}}{b}, \frac{\beta_{SD}}{b}\right)$. Thus, the diversity gain G_1 of the proposed single-hop SATCOM system is given by $G_1 = v_{SD}$.

Similarly, the asymptotic outage probability expression for dual-hop SATCOM system can be obtained as

$$P^{aout}_{DH} = P^{aout}_{SR} + P^{aout}_{RD} - P^{aout}_{SR} P^{aout}_{SR}\,, \tag{40}$$

where individual terms in (40) are given by $P^{aout}_{RD} = F_{\gamma^{asy}_{RD}}(\gamma^f_t)$ and $P^{aout}_{SR} = F_{\gamma^{asy}_{SR}}(\gamma^f_t)\, F_{\gamma^r_{SR}}(\gamma^r_t)$. From (40),

$$\bar{P}_{eSRD} = \int_0^\infty \int_{\gamma_t}^\infty P_{eSRD}(\gamma_{SR}^f, \gamma_{RD}^f) f_{\gamma_{SR}^f}(\gamma_{SR}) f_{\gamma_{RD}^f}(\gamma_{RD})\ d\gamma_{SR}\ d\gamma_{RD}$$
$$+ F_{\gamma_{SR}^f}(\gamma_t) \int_0^\infty \int_0^\infty P_{eSRD}(\gamma_{SR}^r, \gamma_{RD}^f) f_{\gamma_{SR}^r}(\gamma'_{SR}) f_{\gamma_{RD}^f}(\gamma_{RD})\ d\gamma'_{SR}\ d\gamma_{RD}\,, \tag{32}$$

it is observed that $P_{DH}^{aout} \propto (\Gamma_{ii}^f)^{-v_{ii}}$, where $v_{ii} = \min\left(\frac{\zeta_{SR}^2}{b}, \frac{\alpha_{SR}}{b}, \frac{\beta_{SR}}{b}, \frac{\zeta_{RD}^2}{b}, \frac{\alpha_{RD}}{b}, \frac{\beta_{RD}}{b}\right)$. Thus, the diversity gain G_2 of the proposed dual-hop SATCOM system for uplink scenario is given by $G_2 = v_{SR} = \min\left(\frac{\zeta_{SR}^2}{b}, \frac{\alpha_{SR}}{b}, \frac{\beta_{SR}}{b}\right)$, as $\zeta_{SR} < \zeta_{RD}$, $\alpha_{SR} < \alpha_{RD}$, and $\beta_{SR} < \beta_{RD}$.

For the single-hop hybrid FSO/RF SATCOM system, the asymptotic expression for average SEP $\bar{P}_{eSD}$, when $\Gamma_{SD}^f \to \infty$, is given by

$$\bar{P}_{eSD}^a \approx B_{SD}^{af}(\gamma_t^f) + F_{\gamma_{SD}^{asy}}(\gamma_t^f)\, B_{SD}^r\,, \tag{41}$$

where $F_{\gamma_{SD}^{asy}}(\gamma_t^f)$ is given by (39). The expression for $B_{SD}^{af}(\gamma_t^f)$ is given by

$$B_{SD}^{af}(\gamma_t^f) = I_1^a + I_2^a(\gamma_t^f)\,, \tag{42}$$

The closed-form asymptotic expressions for I_1^a and $I_2^a(\gamma_t^f)$ are given in Appendix C.

It is to be noted that B_{SD}^r for a given average SNR of RF link is constant and will not affect the diversity gain. From (41), it is observed that $\bar{P}_{eSD}^a \propto (\Gamma_{SD}^f)^{-v_{SD}}$. Thus, the diversity gain G_1 of single-hop hybrid FSO/RF SATCOM system for a constant average SNR of RF link is given by $G_1 = v_{SD}$.

Similar to single-hop system, we can also obtain the diversity gain of SAGIN-based dual-hop system. The end-to-end asymptotic expression for SAGIN-based dual-hop system is given by

$$\bar{P}_{eSRD}^a = \bar{P}_{eSR}^a + \bar{P}_{eRD}^a - \bar{P}_{eSR}^a\, \bar{P}_{eRD}^a\,. \tag{43}$$

The asymptotic SEP expression for $\bar{P}_{eRD}$ when $\Gamma_{RD}^f \to \infty$ is given by (60) by replacing $\mathcal{F}_{SD}$, $\mathcal{E}_{SD}^{i,x}$, and D_{SD} with $\mathcal{F}_{RD}$, $\mathcal{E}_{RD}^{i,x}$, and D_{RD}, respectively. The asymptotic SEP expression for hybrid FSO transmission over source-to-relay link i.e. $\bar{P}_{eSR}^a$ when $\Gamma_{SR}^f \to \infty$ is obtained similar to (41) by replacing the appropriate source-to-destination FSO link parameters with source-to-relay FSO link parameters and can be written as

$$\bar{P}_{eSR}^a \approx B_{SR}^{af}(\gamma_t) + F_{\gamma_{SR}^{asy}}(\gamma_t^f)\, B_{SR}^r\,. \tag{44}$$

It is observed from the derived expression that $\bar{P}_{eSRD} \propto (\Gamma_{SR}^f)^{-v_{SR}}$. Thus, the diversity gain G_2 of SAGIN-based dual-hop uplink system is given by $G_2 = v_{SR}$.

Note that the asymptotic analysis has been carried out for a fixed average SNR value of RF link and under the condition that the average SNR of FSO link alone tending to infinity. Hence, only coding gain due to RF link has been obtained and the diversity gain obtained from hybrid FSO/RF system remains the same as that of FSO system. The asymptotic analysis for the scenario when both the average SNR of RF and FSO links tending to infinity is given as follows: The asymptotic average SEP of RF link is obtained under the condition that Γ_{jj}^r, where $jj \in \{SR, RD\}$, tends to infinity. After applying [43, Eq.(4.1.18)], high-SNR approximations, and considering only the dominant term in (30), the final simplified asymptotic SEP expression is given by

$$B_{jj}^{ar} = \left(\frac{A\alpha_1 \Omega_{jj} \psi(0) \Gamma(3/2)}{2\sqrt{\pi} B^2}\right) (\Gamma_{jj}^r)^{-1} \tag{45}$$

By substituting (45) in place of B_{SR}^r and B_{SD}^r in (44) and (41), respectively, and assuming $\Gamma_{jj}^r = \Gamma_{ii}^f$, the diversity gain values G_1' and G_2' for single-hop and dual-hop SATCOM systems will be equal to $\min\left(\frac{\zeta_{SD}^2}{b} + 1, \frac{\alpha_{SD}}{b} + 1, \frac{\beta_{SD}}{b} + 1\right)$ and $\min\left(\frac{\zeta_{SR}^2}{b} + 1, \frac{\alpha_{SR}}{b} + 1, \frac{\beta_{SR}}{b} + 1\right)$. It is to be noted that G_1' and G_2' are the highest/full diversity gain values that can be obtained from the proposed single-hop and dual-hop system models.

TABLE II
SIMULATION PARAMETERS

Wave length λ	1550 nm
HAPS altitude H_p	20 Km
LEO satellite altitude H_s	620 Km
GS aperture height H_0	1 m
Pointing error coefficient	$\zeta_{SR} = 5.2$ and ζ_{RD} = 13.07
Variance of background noise (AWGN)	$(\sigma_{SR}^f)^2 = 1.445\times10^{-25}$ A^2/Hz, $(\sigma_{SD}^f)^2 = 4.435 \times 10^{-28}$ A^2/Hz, and $(\sigma_{RD}^f)^2 = 4.435 \times 10^{-28}$ A^2/Hz
Transmit telescope gain	$G_{Tg}^f = G_{Th}^f = 5$ dB
Receive telescope gain	$G_{Rh}^f = G_{Rs}^f = 10$ dB
Zenith angle θ	(a) 80 ° (b) 50 ° (c) 40 °
Wind velocity w	(a) 31 m/s (b) 21 m/s (c) 11 m/s
Beam radius at transmitter W_0^{ii}	2 cm
Phase front radius of curvature of transmitter beam F_0	∞
Heavy Shadowing	$b_1 = 0.063$, $m_1 = 1$, $\Omega_1 = 0.0007$
Moderate Shadowing	$b_1 = 0.251$, $m_1 = 5$, $\Omega_1 = 0.279$
Light Shadowing	$b_1 = 0.158$, $m_1 = 19$, $\Omega_1 = 1.29$
RF carrier frequency	f_r = 5 GHz
Optical to electrical conversion coefficient	$\eta_{ii} = 0.8$
RF antenna gains	$G_T = 28$ dB and $G_R = 10$ dB
RF attenuation losses	L_R = 0.01 dB/Km (No rain), L_A = 5.4 $\times10^{-3}$ dB/km, and $L_O = 2$ dB
Receiver Noise Bandwidth (RF)	BW = 74.8 dBHz
System noise temperature, 58K	$T_N = 17.6$ dBK
Noise figure	$N_F = 2$ dB

IV. NUMERICAL RESULTS AND DISCUSSIONS

The parameters assumed in our simulation studies are shown in Table II [31], [32]. As the link between HAPS and satellite is not very sensitive to channel distortions, we assume $\Gamma_{RD}^f = 5 \times \Gamma_{SR}^f$, very weak turbulence and negligible

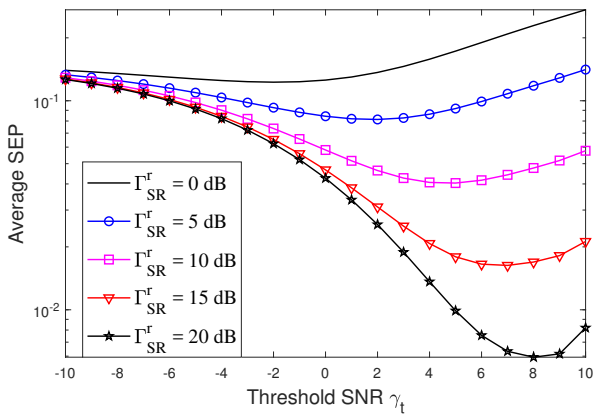

Fig. 2. Average SEP versus threshold SNR for different values of average SNR of RF link

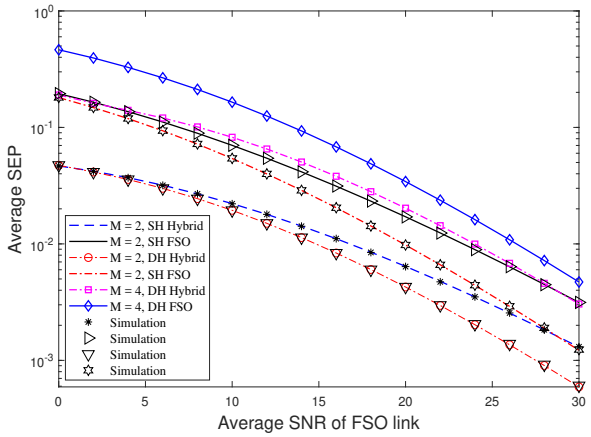

Fig. 3. Performance of different system models for uplink scenario

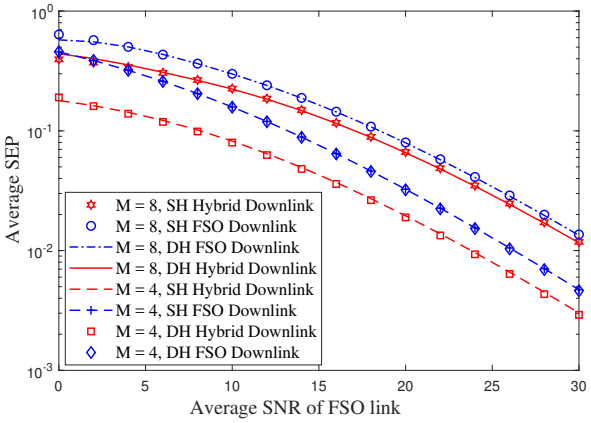

Fig. 4. Performance of different system models for downlink scenario

pointing errors scenario (i.e. $\zeta_{RD} = 13.07$). Moreover, for simplicity, we assume $\theta = \theta_p = \theta_S = \theta_H$, where θ_S and θ_H are the zenith angles that indicate the angle between the zenith and the propagation orientation from HAPS-to-satellite and GS-to-HAPS, respectively. Similarly, θ_p denotes the angle between the zenith and the propagation orientation from GS-to-satellite. However, we have also relaxed the equal zenith angle assumption in Fig. 8. Also, we have assumed IM/DD scheme in our simulation studies except Fig. 8. The summation limits in (59) and (31) are truncated to $k=50$ and $n=10$, as $k > 50$ and $n > 10$ do not have an impact on the fifth decimal figure of the average SEP values. Further, the typical range of HAPS altitude adopted for simulation is 20 km as shown in Table II. It is motivated by the facts which are given as follows: (a) The atmospheric turbulence effects on an optical beam is less severe at the height of 20 Km than directly above ground. (b) As wind speed is very less in these altitudes, HAPS requires only less power to maintain its position. (c) Large coverage area for telecommunications is possible at these altitudes. (d) HAPS is situated above normal commercial airline traffic. The commercial planes usually operate at an altitude much lower than the altitude of HAPS. A circular polarization either right-hand circular polarization or left-hand circular polarization is used for RF channel [44]. A moderate-gain omnidirectional terminal is considered as the HAPS terminal segment and the RF antenna pattern is assumed to be omnidirectional for the azimuth and partially omnidirectional for the elevation [44].

In Fig. 2, the variation of average SEP of hybrid FSO/RF systems with respect to switching threshold SNR γ_t is shown, respectively, for different values of average SNR of RF links Γ^r_{SR} assuming heavy shadowing, $w = 21$m/s, $\theta = 80°$, and $M = 4$. It is noticed that the average SEP value is minimum at γ_t =[-2 2 5 7 8] dB for Γ^r_{SR} =[0 5 10 15 20] dB. In addition, the optimal threshold value remains same irrespective of the average SNR of FSO links. The optimum threshold SNR values γ_t^{opt} are the corresponding γ_t^f values for which the average SEP performance curve reaches minimum. It is inferred that with the availability of better RF link (i.e. RF link with high average SNR), the optimum switching threshold SNR γ_t^{opt} to switch from FSO to RF link also increases. The main reason behind this phenomenon is given as follows: When the average SNR value of RF link increases or when the quality of available RF link is good, then to achieve minimum probability the optimum threshold value should increase. This is because, as the optimum threshold value increases, the FSO system will be in outage frequently and RF link will be used with higher probability which in turn improves the overall performance by nullifying the FSO channel distortions. Therefore, when the average SNR of RF link is constant, then irrespective of the average SNR of FSO link, the optimum threshold value should remains same to achieve minimum average SEP.

In Fig. 3, the average SEP performance comparison of single-hop FSO system, single-hop hybrid FSO/RF system, dual-hop FSO system, and dual-hop hybrid FSO/RF system with respect to average SNR of FSO links is shown assuming average shadowing, zenith angle $\theta = 80°$, wind velocity $w =$ 21m/s, $\gamma_t^f = \gamma_t^{\text{opt}}$, and $\Gamma^r_{jj} = 5$ dB, where $jj \in \{SR, SD\}$. Firstly, it is observed that the analytical results match exactly with the Monte-Carlo simulations and performance deteriorates with increase in M as expected. The hybrid FSO/RF

system (both single-hop and dual-hop) performs better than the FSO system with a coding gain of more than 5 dB at the SEP value of 10^{-2} with a moderate average SNR of RF link (i.e. $\Gamma_{ii}^{r} = 5$ dB). Thus, increase in coding gain is obtained due to backup RF link. Most importantly, it has been observed that the dual-hop FSO system performs better than the single-hop FSO system with a coding gain of 4 dB. In addition, the dual-hop hybrid system performs better than the single-hop hybrid system with a coding gain of around 2 dB. Thus, significant improvement in the SEP performance and diversity gain have been obtained by deploying HAPS for uplink scenario. As FSO link is prone to beam-wander induced pointing errors in case of uplink scenario, the deployment of HAPS helps in counteracting the pointing errors. Moreover, the diversity improvement is due to the following reason: With decrease in link distance due to deployment of HAPS in case of dual-hop scenario compared to single-hop scenario, the Rytov variance decreases and the small and large scale turbulence parameters increases. Since the diversity order depends on the turbulence parameters, improvement in diversity gain is obtained in case of dual-hop scenario compared to single-hop scenario.

In addition, the performance improvement of dual-hop scenario with HAPS compared to single-hop scenario is also due to the following reason: In case of uplink scenario, the FSO signal first travels from GS to HAPS, which is highly sensitive to both beam scintillation and misalignment errors, as the beam size of the FSO signal is much smaller than the turbulent eddy size in the atmosphere. At HAPS, both the atmospheric turbulence effects are nullified and then the FSO signal is forwarded to satellite. For the single-hop scenario, both the turbulence effects are not nullified, as HAPS is not utilized. Hence, the FSO signal suffers from loss of SNR and pointing errors in case of uplink scenario and the utilization of HAPS leads to better system performance in case of dual-hop system compared to single-hop system.

However, no improvement in the performance of the dual-hop system is noticed compared to single-hop system for downlink scenario as shown in Fig. 4. This is due to the fact that in the case of downlink scenario, the optical signal undergoes less attenuation when it travels from satellite to HAPS, as satellite-to-HAPS link is less prone to varying weather conditions. Thus, it suffers low beam divergence till it reaches the height at which the HAPS is stationed. When the optical signal travels from HAPS to GS during the orthogonal phase, it enters the high attenuation region and suffers high beam divergence, which will be approximately same as that of the beam divergence encountered by the optical signal during single-hop downlink transmission. Thus, no performance improvement is achieved due to HAPS in case of dual-hop system with respect to single-hop system unlike uplink scenario. Hence, we are mainly interested in the trends of the uplink scenario compared to downlink scenario in our proposed work. The expression to calculate large scale turbulence parameter α_{ii} is different for downlink scenario and the same is given in [9, Eq.(9)].

In Fig. 5, the SEP performances of single-hop and dual-hop

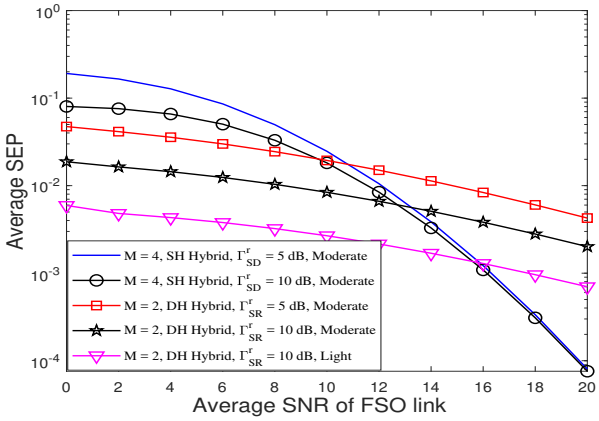

Fig. 5. SEP performance of hybrid systems considering different values of average SNR of RF link

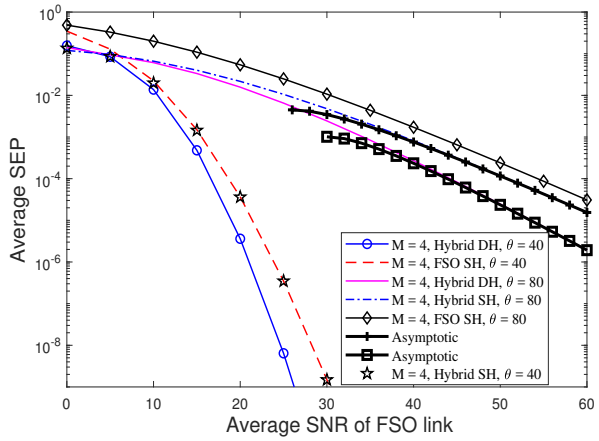

Fig. 6. SEP performance of hybrid SATCOM systems considering different zenith angle values

hybrid systems are shown for different values of average SNR of RF link and shadowing severity. It is inferred that increase in average SNR of RF link (from 5 dB to 10 dB) and decrease in shadowing severity improve the performance of single-hop and dual-hop hybrid systems.

In Fig. 6, the SEP performances of single-hop and dual-hop hybrid FSO/RF system are shown for two different values of zenith angle θ assuming light shadowing, $\Gamma_{SR}^{r} = 8$ dB and 5 dB, $w = 21$m/s, $M = 4$, and $\gamma_t^f = \gamma_t^{\text{opt}}$. It is observed from the performance that decrease in the zenith angle improves the SEP performance. Note that with decrease in zenith angle, the Rytov variance [21] decreases and the small and large scale turbulence parameters (i.e. α_{ii} and β_{ii}) increases. As the diversity order of the proposed system depends on α_{ii} and β_{ii}, significant improvement in the SEP performance in terms of diversity gain is obtained with decrease in zenith angle. Otherwise, the propagation distance of the optical beam increases with increase in zenith angle leaving it more vulnerable to free space loss, atmospheric turbulence, beam wander, atmospheric attenuation due to varying weather conditions, pointing errors, and RF fading effects, compared to the

scenario with low zenith angle value. Therefore, significant degradation in the performance is noticed with increase in zenith angle value. Since the diversity gain of the system also depends on atmospheric turbulence and pointing errors parameters, increase in zenith angle also affects the diversity gain of the system.

However, the coding gain of dual-hop and single-hop hybrid FSO/RF systems compared to FSO systems deteriorate with decrease in zenith angle. As shown in the figure, coding gain value of more than 5 dB is obtained from hybrid system compared to FSO system for the case when $\theta = 80°$. However, the SEP performances of FSO and hybrid FSO/RF systems are almost equal for $\theta = 40°$ as shown in Fig. 5. Thus, backup RF link helps in enhancing the reliability for worst case scenario with high zenith angle values. It is also noticed that the asymptotic SEP values almost match the exact SEP values in the high-SNR region for the case when the average SNR of RF link remains constant, which validates the fact that the diversity order of the proposed system is min $\left(\frac{\zeta_{ii}^2}{b}, \frac{\alpha_{ii}}{b}, \frac{\beta_{ii}}{b}\right)$, where $ii = \{SR\}$ and $ii = \{SD\}$ for dual-hop and single-hop scenarios, respectively.

Similarly, asymptotic SEP curve almost matches the exact SEP curve in the high-SNR region for the case when the average SNR of RF link also varies with the average SNR of FSO link (i.e. $\Gamma_{jj}^r = \Gamma_{ii}^f$). Thus, it is inferred that full diversity gain due to both FSO and RF links, which is equal to min $\left(\frac{\zeta_{ii}^2}{b} + 1, \frac{\alpha_{ii}}{b} + 1, \frac{\beta_{ii}}{b} + 1\right)$, can be obtained for the case when the average SNR of RF link also varies with the average SNR of FSO link under the condition $\gamma_t^f = \gamma_t^{\text{opt}}$. Further, if the average SNR of RF link is constant, then only coding gain will be obtained due to backup RF link and the diversity gain of hybrid FSO/RF system will be equal to diversity gain of FSO system. This is because, for the case when the average SNR of RF link Γ_{jj}^r is constant, the optimum switching threshold SNR value γ_t^{opt} is also fixed. Further, for high-SNR region (i.e. $\Gamma_{ii}^f >> \gamma_t^{\text{opt}}$), it is least likely that the instantaneous SNR of FSO link falls below fixed γ_t^{opt} and the FSO link will be active most of the time. Therefore, only FSO link contributes to the diversity gain of hybrid FSO/RF system. However, for the case when the average SNR of RF link also varies with the average SNR of FSO link, the optimum switching threshold also increases with Γ_{jj}^r as inferred from Fig. 2. So the probability that the instantaneous SNR of FSO link falls below increasing γ_t^{opt} or the probability of usage of RF link is higher compared to the previous case especially in the high-SNR region. Thus, both FSO and RF links contribute in the diversity gain of the hybrid FSO/RF system, which validates the derived full diversity gain.

In Fig. 7, the SEP performances of the dual-hop FSO and hybrid FSO/RF systems are compared for different values of w assuming heavy shadowing, $\Gamma_{SR}^r = 5$ dB, $\theta = 80°$, $\gamma_t^f = \gamma_t^{\text{opt}}$, and $M = 2$. It is inferred from the figure that increase in wind velocity w degrades the performance of both FSO and hybrid FSO/RF systems. This is due to the fact

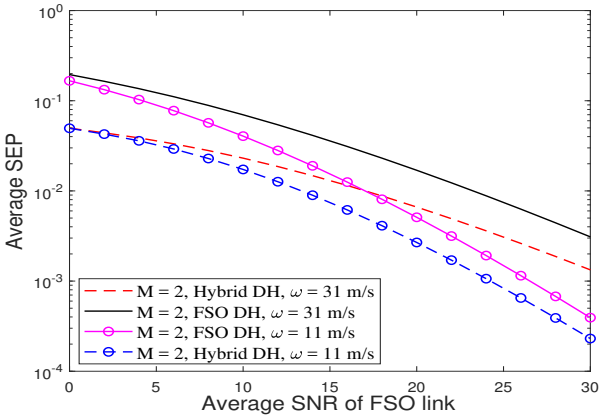

Fig. 7. SEP performance of FSO and hybrid SATCOM systems considering different values of wind velocity

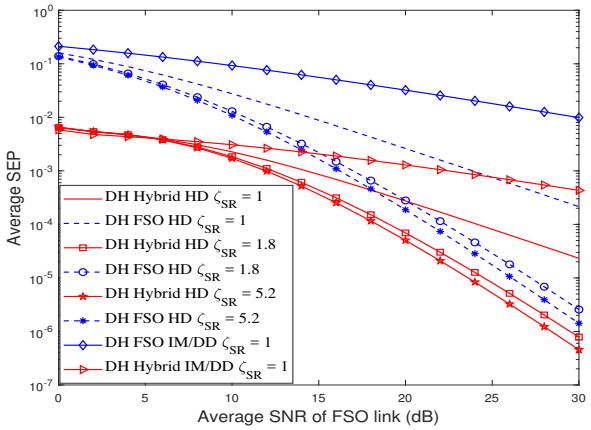

Fig. 8. SEP performance of FSO and hybrid SATCOM systems considering different values of pointing error coefficient

that the increase in wind velocity increases the formation of vortexes in air. This phenomenon will effectively change the refractive index of the medium, which will cause beam wander induced pointing errors and higher fluctuations in the received signal amplitude. Thus, degradation in the average SEP performance is observed from the trends. Most importantly, it is also observed that the wind velocity impacts the performance of FSO system to a great extent compared to hybrid FSO/RF system. Hence, reliable RF backup link has reduced the impact of wind velocity on the system performance.

Fig. 8 shows the effect of pointing errors on the dual-hop SATCOM system performance by varying the pointing errors coefficient ζ_{SR} assuming heterodyne detection scheme, $\zeta_{RD} = 6$, $\Gamma_{SR}^r = 10$ dB, $\theta_H = 80°$, $\theta_S = 40°$, $\gamma_t^f = \gamma_t^{\text{opt}}$, $M = 2$, and light shadowing scenario. Sine the zenith angle values are different for HAPS-to-satellite and GS-to-HAPS links, the assumption of HAPS being in a straight-line path from GS-to-satellite is relaxed for this scenario. The performance is shown for three different values of ζ_{SR}, which are given by $\zeta_{SR} = 1, 1.8$, and 5.2. It is to be noted that the severity of pointing errors is high for lower values of ζ_{SR}. In addition, as HAPS-to-Satellite FSO link is less sensitive

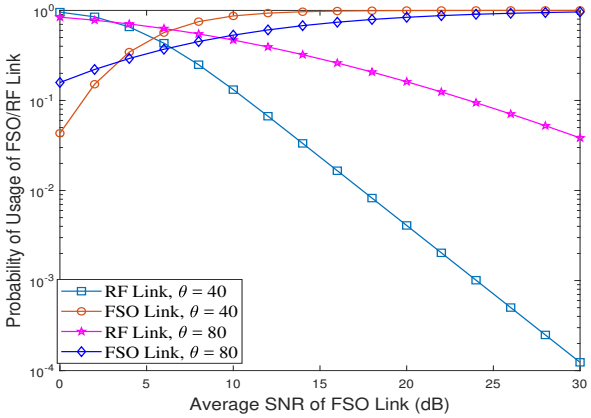

Fig. 9. Probability of usage of RF/FSO link for different values of zenith angle

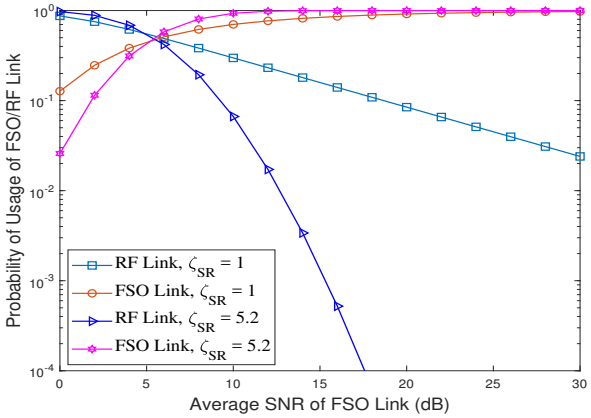

Fig. 10. Probability of usage of RF/FSO link for different values of pointing error coefficient

to pointing errors, high value of pointing errors coefficient is assumed in our simulations. From Fig. 8, it is observed that to achieve the average SEP value of 10^{-3}, the coding gain values obtained using dual-hop hybrid FSO/RF SATCOM system over dual-hop FSO SATCOM system are 10 dB, 5 dB, and 3.5 dB for $g = 1, 1.8,$ and 5.2, respectively. Thus, it is observed that the backup RF link provides better coding gain when the severity of pointing errors is high. Further, improvement in the performance of heterodyne detection scheme is noticed due to its coherent detection nature as compared to IM/DD scheme.

It is to be noted that the hybrid FSO/RF system provides much better coding gain under the conditions with high pointing errors, more propagation distance (i.e. high zenith angle value), and high wind velocity as compared to low pointing errors, less propagation distance, and low wind velocity conditions as discussed before. This is because, the probability of usage of RF link is high under the conditions in which the FSO link is more prone to channel distortions. Further, the probability of switching to RF link is comparatively less or the probability of usage of FSO link is high under the conditions with less FSO channel distortions. Hence, high coding gain due to backup RF link is observed. The above inferences are also justified from the trends shown using probability of usage

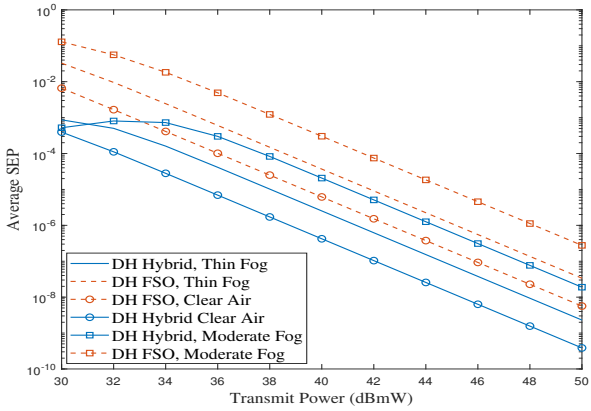

Fig. 11. SEP performance of DH FSO and hybrid SATCOM systems assuming different weather conditions

of FSO or RF link in Fig. 9 and Fig. 10. Here, the probability of usage of RF and FSO link is evaluated from the outage and non-outage probabilities of FSO link, respectively. From both the figures, it has been observed that the probability of usage of RF link is higher for the scenarios with high pointing errors and zenith angle values compared to the scenarios with low pointing errors and zenith angle values especially for average SNR values greater than 5 dB.

In Fig. 11, the average SER plots of dual-hop SATCOM system with respect to FSO transmit power are shown for various weather conditions. Here, we consider three scenarios of weather condition (i.e. clear air, thin or light fog, and moderate fog) for both dual-hop FSO and hybrid FSO/RF SATCOM systems. The parameters assumed in the simulations are listed in Table II. In addition, the RF transmit power assumed in our simulations is $p_g^r = 40$dBm. Further, the atmospheric transmittance values I_l^{SR} for clear air, thin or light fog, and moderate fog conditions according to MODTRAN 4.0 simulations [40] based on visibility [20] are assumed as 0.9, 0.52 and 0.15, respectively. It is observed that the dual-hop hybrid SATCOM system performs better under all scenarios compared to dual-hop FSO system due to backup RF links. The coding gain offered by hybrid FSO/RF system over FSO system to achieve the average SER of 10^{-4} is found to be around 4 dBm. Interestingly, it is also inferred that dual-hop hybrid FSO/RF system under moderate fog scenario performs slightly better than dual-hop FSO system under light fog scenario. Similarly, improvement in the performance is also observed in case of dual-hop hybrid FSO/RF system under light fog scenario compared to dual-hop FSO system under clear air scenario.

In Fig. 12, the outage performance comparison of different system models with respect to average SNR of FSO links is shown assuming average shadowing, zenith angle $\theta = 80°$, wind velocity $w = 21$m/s, and $\gamma_t^f = \gamma_t^r = 5$ dB for different values of average SNR of RF links. It is observed from the plots that the theoretical outage probability values exactly match with the simulated outage values. It is also noticed from the outage performance curves that the hybrid FSO/RF

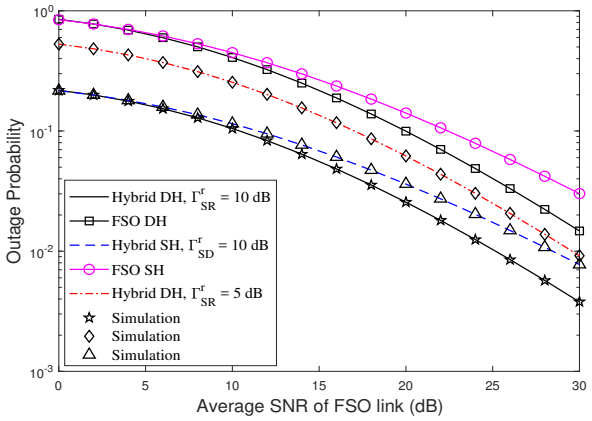

Fig. 12. Outage performance comparison of different system models

systems performs better than the FSO systems. Hence, the backup RF link helps in improving the outage performance of FSO links. In addition, outage performance improvement is noticed especially in the high-SNR region for dual-hop FSO and hybrid systems compared to single-hop FSO and hybrid systems, respectively.

V. Conclusions

In this paper, we proposed two system models for uplink SATCOM scenario namely SAGIN-based hybrid FSO/RF communication using HAPS (i.e. dual-hop scenario) and single-hop hybrid FSO/RF SATCOM to counteract atmospheric turbulence effects and improve link reliability of FSO-based SATCOM. The exact expressions for the average SEP and outage probability were derived in closed-form assuming Gamma-Gamma fading turbulence with pointing errors for FSO links and Shadowed-Rician fading for RF link. In addition, closed-form asymptotic expressions with less computational complexity were also derived and the diversity gain was obtained. The derived expressions were validated using Monte-Carlo simulations. From the performance plots, it was observed that the hybrid FSO/RF systems perform better than the FSO systems due to backup RF link. In addition, the utilization of HAPS as a relay station also improved the reliability of uplink SATCOM. Moreover, when zenith angle, severity of pointing errors, and wind velocity increases, it was observed that the coding gain obtained due to RF link increases. Finally, a numerical optimization was performed to obtain the optimal threshold value of the proposed system.

Appendix A
Meijer G-function

The primary definition for Meijer G-function is given by

$$G_{p\ q}^{m\ n}\left(z\middle|\begin{matrix}a_1,a_2,\cdots,a_n,\cdots,a_p\\ b_1,b_2,\cdots b_m,\cdots,b_q\end{matrix}\right)=\frac{1}{2\pi i}\int\frac{\left(\prod_{k=1}^{m}\Gamma(s+b_k)\right)\prod_{k=1}^{n}\Gamma(1-a_k-s)}{\left(\prod_{k=n+1}^{p}\Gamma(s+a_k)\right)\prod_{k=m+1}^{q}\Gamma(1-b_k-s)}z^{-s}ds\,, \tag{46}$$

where $0\leq m\leq q$, $0\leq n\leq p$, $m\in\mathbb{N}$, and $n\in\mathbb{N}$.

The following are some important equations related to Meijer G-function, which are used in our derivation. The relation between Meijer G-function and erfc$(\cdot)$ is given by

$$G_{1\ 2}^{2\ 0}\left(z\middle|\begin{matrix}a\\ a-1,a-\frac{1}{2}\end{matrix}\right)=\sqrt{\pi}z^{a-1}erfc(\sqrt{z}) \tag{47}$$

The relation between Meijer G-function and modified Bessel function of second kind $K_v(\cdot)$ is given by

$$G_{0\ 2}^{2\ 0}\left(z\middle|\begin{matrix}-\\ b,c\end{matrix}\right)=2z^{\frac{b+c}{2}}K_{b-c}(2\sqrt{z}) \tag{48}$$

Appendix B
Uplink Turbulence Parameters

The uplink turbulence parameter α_{SR} is given by (49), which is shown on the top of next page, and β_{SR} for GS-to-HAPS link is given by [20]

$$\beta_{SR}=\left[\exp\left(\frac{0.51(\sigma_{SR})^2}{(1+0.69(\sigma_{SR})^{12/5})^{5/6}}\right)-1\right]^{-1}, \tag{50}$$

In (49) and (50), Rytov variance, which is denoted by $(\sigma_{SR})^2$, for the slant optical path from GS-to-HAPS link is given by

$$\begin{aligned}(\sigma_{SR})^2 &= 2.25k_1^{\frac{7}{6}}(H_p-H_0)^{\frac{5}{6}}\sec^{\frac{11}{6}}(\theta_H)\\ &\times\int_{H_0}^{H_p}C_n^2(h)\left(1-\frac{h-H_0}{H_p-H_0}\right)^{\frac{5}{6}}\left(\frac{h-H_0}{H_p-H_0}\right)^{\frac{5}{6}}dh\,.\end{aligned} \tag{51}$$

Using the Hufnagel-Valley (H-V) boundary model, the refractive index structure parameter $C_n^2(h)$ is given by [21] [8]

$$\begin{aligned}C_n^2(h) &= 0.00594\left(\frac{w}{27}\right)^2(10^{-5}h)^{10}\exp\left(\frac{-h}{1000}\right)\\ &+2.7\times10^{-16}\exp\left(\frac{-h}{1500}\right)+C_n^2(0)\exp\left(\frac{-h}{100}\right),\end{aligned} \tag{52}$$

where ground level turbulence $C_n^2(0)$, which is equal to $1.7\times10^{-14}\mathrm{m}^{-2/3}$.

In (49), W_0^{SR} denotes the beam size at the transmitter and W^{SR} denotes the beam size at the receiver, which is given by $W^{SR}=W_0^{SR}\sqrt{\Theta_{SR}^2+\Lambda_{SR}^2}$. Note that Θ_{SR} and Λ_{SR} are the beam parameters at the transmitter, which are given by $\Lambda_{SR}=\frac{2L_p}{k_1(W_0^{SR})^2}$ and $\Theta_{SR}=1-L_p/F_0$, respectively. Further, F_0 is the phase front radius of curvature of the beam at the transmitter and L_p denotes the transmission distance between HAPS and GS, which can be written as $L_p=H_p/cos(\theta_H)$. In addition, r_{SR} indicates the fried parameter, which is given by

$$r_{SR}=\left[0.42\sec(\theta_H)k_1^2\int_{H_0}^{H_p}C_n^2(h)dh\right]^{\frac{-3}{5}} \tag{53}$$

Moreover, $\Delta_{pe}^{SR}=\frac{\sigma_{pe}^{SR}}{L_p}$ in (49) denotes the beam-wander induced pointing errors. The beam-wander induced pointing errors variance $(\sigma_{pe}^{SR})^2$ is given by

$$\begin{aligned}(\sigma_{pe}^{SR})^2 &= 0.54(H_p-H_0)^2\sec^2(\theta_H)\left(\frac{\lambda}{2W_0^{SR}}\right)^2\\ &\times\left(\frac{2W_0^{SR}}{r_{SR}}\right)^{\frac{5}{3}}\left[1-\left(\frac{C_r^2(W_0^{SR})^2/r_{SR}^2}{1+C_r^2(W_0^{SR})^2/r_{SR}^2}\right)\right],\end{aligned} \tag{54}$$

$$\alpha_{SR} = 5.95(H_p - H_0)^2 \sec^2(\theta_H) \left(\frac{2W_0^{SR}}{r_{SR}}\right)^{5/3} \left(\frac{\Delta_{pe}^{SR}}{W^{SR}}\right)^2 + \left[\exp\left(\frac{0.49(\sigma_{SR})^2}{(1+0.56(\sigma_{SR})^{12/5})^{7/6}}\right) - 1\right]^{-1}, \quad (49)$$

where C_r is a scaling constant, which is assumed as 2π.

The uplink turbulence parameter α_{RD} is modelled similar to (49) by replacing $(H_p - H_0)^2$, θ_H, W_0^{SR}, r_{SR}, Δ_{pe}^{SR}, and σ_{SR} with $(H_s - H_p)^2$, θ_S, W_0^{RD}, r_{RD}, Δ_{pe}^{RD}, and σ_{RD}. Here, the beam size at the receiver is given by $W^{RD} = W_0^{RD}\sqrt{\Theta_{RD}^2 + \Lambda_{RD}^2}$, where $\Lambda_{RD} = \frac{2L_s}{k_1(W_0^{RD})^2}$, $\Theta_{RD} = 1 - L_s/F_0$, and L_s denotes the transmission distance between satellite and HAPS, which is given by $L_s = (H_s - H_p)/cos(\theta_S)$. Another parameter β_{RD} for HAPS-to-satellite link is modelled similar to GS-to-HAPS link by replacing $(\sigma_{SR})^2$ with $(\sigma_{RD})^2$, which denotes the Rytov variance from HAPS-to-satellite link and is given by

$$(\sigma_{RD})^2 = 2.25k_1^{\frac{7}{6}}(H_s - H_p)^{\frac{5}{6}} \sec^{\frac{11}{6}}(\theta_S) \times \int_{H_p}^{H_s} C_n^2(h) \left(1 - \frac{h - H_p}{H_s - H_p}\right)^{\frac{5}{6}} \left(\frac{h - H_p}{H_s - H_p}\right)^{\frac{5}{6}} dh\,. \quad (55)$$

The fried parameter r_{RD} is given by

$$r_{RD} = \left[0.42\sec(\theta_S)k_1^2 \int_{H_p}^{H_s} C_n^2(h)dh\right]^{\frac{-3}{5}} \quad (56)$$

The beam-wander induced pointing errors can be written as $\Delta_{pe}^{RD} = \frac{\sigma_{pe}^{RD}}{L_s}$. Further, the beam-wander induced pointing error variance $(\sigma_{pe}^{RD})^2$ is given by (54) by replacing $(H_p - H_0)^2$, θ_H, W_0^{SR}, r_{SR} with $(H_s - H_p)^2$, θ_S, W_0^{RD}, and r_{RD}, respectively.

For uplink scenario during single-hop transmission, the turbulence parameter α_{SD} is obtained by replacing corresponding terms in (49) with source-to-destination link terms, where $W^{SD} = W_0^{SD}\sqrt{\Theta_{SD}^2 + \Lambda_{SD}^2}$, $\Lambda_{SD} = \frac{2L}{k_1(W_0^{SD})^2}$, $\Theta_{SD} = 1 - L/F_0$, and L denotes the transmission distance between satellite and GS, which is given by $L = (H_s - H_0)/cos(\theta_S)$. Another parameter β_{SD} is given by (50) by replacing $(\sigma_{SR})^2$ with $(\sigma_{SD})^2$, which denotes the Rytov variance from GS-to-satellite. The Rytov variance can be written similar to (51) by replacing H_p and θ_H with H_s and θ_p. Similarly, the fried parameter r_{SD} and the beam-wander induced pointing error variance $(\sigma_{pe}^{SD})^2$ parameter during SH transmission are modelled by changing appropriate parameters.

APPENDIX C
AVERAGE AND ASYMPTOTIC SEP DERIVATIONS

Here, we derive the closed-form expressions for I_1 and $I_2(\gamma_t^f)$ in (29). After substituting (17) and (25) in I_1 and simplifying the resultant expression using [34, eq.(07.34.21.0013.01)], the final expression in closed-form is given by

$$I_1 = \frac{A\mathcal{F}_{SD}}{2\sqrt{\pi}}\, G_{\,b+2\;\;3b+1}^{\,3b\;\;2} \left(\frac{(D_{SD})^b}{b^{2b}B^2\,\Gamma_{SD}^f}\middle| \begin{matrix}1, 1/2, \mathcal{E}_{SD}^1 \\ \mathcal{E}_{SD}^2, 0\end{matrix}\right). \quad (57)$$

In (29), the expression for $I_2(\gamma_t^f)$ after substituting (26) can be re-written as

$$I_2(\gamma_t^f) = \int_0^{\gamma_t^f} \frac{A}{2} f_{\gamma_{SD}^f}(\gamma_{SD})d\gamma_{SD} - \int_0^{\gamma_t^f} \left(\frac{2}{\sqrt{\pi}} \times \sum_{k=0}^{\infty} \frac{(-1)^k(\gamma_{ii})^{\frac{2k+1}{2}} B^{2k+1}}{k!(2k+1)}\right) f_{\gamma_{SD}^f}(\gamma_{SD})d\gamma_{SD}\,, \quad (58)$$

After substituting (17) in (58), the final expression can be obtained using [34, eq.(07.34.21.0084.01)] and is given by

$$I_2(\gamma_t^f) = \frac{AF_{\gamma_{ii}^f}(\gamma_t^f)}{2} - \frac{A\mathcal{F}_{SD}}{\sqrt{\pi}} \sum_{k=0}^{\infty} \frac{(-1)^k\, B^{2k+1}(\gamma_t^f)^{(k+1/2)}}{k!\,(2k+1)} \times G_{\,b+1\;\;3b+1}^{\,3b\;\;1} \left(\frac{(D_{SD})^b\gamma_t^f}{b^{2b}\Gamma_{SD}^f}\middle| \begin{matrix}(1-k-1/2), \mathcal{E}_{SD}^1 \\ \mathcal{E}_{SD}^2, (-k-1/2)\end{matrix}\right). \quad (59)$$

The asymptotic expressions for (57) and (59), which are denoted as I_1^a and $I_2^a(\gamma_t^f)$ are given as follows: The asymptotic expression I_1^a, when $\Gamma_{SD}^f \to \infty$, is obtained by applying [34, eq.(07.34.06.0040.01)] on (57) and is given by

$$I_1^a \approx \frac{A\mathcal{F}_{SD}}{2\sqrt{\pi}} \sum_{l=1}^{3b} \frac{\Gamma(\mathcal{E}_{SD}^{2,l} + \frac{1}{2}) \prod_{\substack{x=1 \\ x\neq l}}^{3b} \Gamma(\mathcal{E}_{SD}^{2,x} - \mathcal{E}_{SD}^{2,l})}{\mathcal{E}_{SD}^{2,l} \prod_{x=1}^{b} \Gamma(\mathcal{E}_{SD}^{1,x} - \mathcal{E}_{SD}^{2,x})} \times \left(\frac{(D_{SD})^b}{b^{2b}B^2\,\Gamma_{SD}^f}\right)^{\mathcal{E}_{SD}^{2,l}} \quad (60)$$

Now the asymptotic expression $I_2^a(\gamma_t^f)$, when $\Gamma_{SD}^f \to \infty$, is obtained by applying [34, eq.(07.34.06.0040.01)] on (59) and the same can be written as

$$I_2^a(\gamma_t^f) \approx \frac{AF_{\gamma_{SD}^{asy}}(\gamma_t^f)}{2} - \frac{A\mathcal{F}_{SD}}{\sqrt{\pi}} \sum_{k=0}^{\infty} \frac{(-1)^k\, B^{2k+1}(\gamma_t^f)^{(k+1/2)}}{k!\,(2k+1)} \times \sum_{l=1}^{3b} \frac{\prod_{\substack{x=1 \\ x\neq l}}^{3b} \Gamma(\mathcal{E}_{SD}^{2,x} - \mathcal{E}_{SD}^{2,l})}{(\mathcal{E}_{SD}^{2,l} + n + \frac{1}{2}) \prod_{x=1}^{b} \Gamma(\mathcal{E}_{SD}^{1,x} - \mathcal{E}_{SD}^{2,x})} \left(\frac{D_{SD}\gamma_t^f}{b^{2b}\Gamma_{SD}^f}\right)^{\mathcal{E}_{ii}^{2,l}} \quad (61)$$

REFERENCES

[1] D Guha-Sapir, P. Hoyois, and R. Below, "Annual disaster statistical review 2016: The numbers and trends,"Centre for Research on the Epidemiology of Disasters (CRED), Brussels, Oct. 2017, [Online]. Available: https://reliefweb.int/sites/reliefweb.int/files/resources/adsr_2016.pdf.

[2] L. J. Ippolito, *Satellite communications systems engineering: atmospheric effects, satellite link design and system performance* 2nd ed., John Wiley and Sons, Ltd., 2017.

[3] J. Liu, Y. Shi, Z. M. Fadlullah, and N. Kato, "Space-air-ground integrated network: A survey, *IEEE Commun. Surveys Tuts.*, vol. 20, no. 4, pp. 2714–2741, Fourthquarter 2018.

[4] H. Kaushal and G. Kaddoum, "Optical communication in space: challenges and mitigation techniques," *IEEE Commun. Surveys Tuts.*, vol. 19, no. 1, pp. 57-96, Firstquarter 2017.

[5] M.A. Khalighi and M. Uysal, "Survey on free space optical communication: A communication theory perspective, *IEEE Commun. Surveys Tuts.*, vol. 16, no. 4, pp. 2231–2258, June 2014.

[6] C. C-Chen and M. Z. Win, "Frequency noise measurement of diode-pumped Nd:YAG ring lasers," *IEEE Photon. Technol. Lett.*, vol. 2, no. 11, pp. 772–774, Nov. 1990.

[7] M. Z. Win, C. C-Chen, and R. A. Scholtz, "Optical phase-locked loop (OPLL) for an amplitude modulated communications link using solid-state lasers," *IEEE J. Sel. Areas Commun.*, vo. 13, no. 3, pp. 569–576, Apr. 1995.

[8] H. Kaushal, V. K. Jain, and S. Kar, *Free Space Optical Communication*, Springer India, 2017.

[9] J. Ma, K. Li, L. Tan, S. Yu, and Y. Cao, "Performance analysis of satellite-to-ground downlink coherent optical communications with spatial diversity over Gamma-Gamma atmospheric turbulence, *Appl. Opt.*, vol. 54, no. 25, pp. 7575–7585, Sep. 2015.

[10] M. Usman, H.-C. Yang, and M-S. Alouini, "Practical switching-based hybrid FSO/RF transmission and its performance analysis, *IEEE Photon. J.*, vol. 6, no. 5, pp. 1-14, Oct. 2014.

[11] E. Zedini, H. Soury, and M. Alouini, "Dual-hop FSO transmission systems over Gamma-Gamma turbulence with pointing errors, *IEEE Trans. Wireless Commun.*, vol. 16, no. 2, pp. 784–796, Feb. 2017.

[12] J Libich, M. Komanec, S. Zvanove, P. Pesek, WO. Popoola, and Z. Ghassemlooy, "Experimental verification of an all-optical dual-hop 10Gbit/s free-space optics link under turbulence regimes, *Opt. Lett.*, vol. 40, no. 3, pp. 391–394, Feb. 2015.

[13] S. Sharma, A.S.Madhukumar, and Swaminathan R, "Switching-based cooperative decode-and-forward relaying for hybrid FSO/RF networks, *IEEE/OSA J. Opt. Commun. Netw.*, vol. 11, no. 6, pp. 267–281, June 2019.

[14] S. Sharma, A.S.Madhukumar, and Swaminathan R, "Performance of dual-hop hybrid FSO/RF system with pointing errors optimization," *in Proc. IEEE VTC Spring*, Antwerp, Belgium, 2020, pp. 1-5.

[15] F. Fidler, M. Knapek, J. Horwath, and W. R. Leeb, "Optical communications for high-altitude platforms, *IEEE J. Sel. Topics Quantum Electron.*, vol. 16, no. 5, pp. 1058–1070, Sep./Oct. 2010.

[16] S. Karapantazis and F. Pavlidou, "Broadband communications via high-altitude platforms: A survey," *IEEE Commun. Surveys Tuts.*, vol. 7, no. 1, pp. 2-31, First Qtr. 2005.

[17] T. Rakia, H. C. Yang, M. S. Alouini, and F. Gebali, "Outage analysis of practical FSO/RF hybrid system with adaptive combining," *IEEE Commun. Lett.*, vol. 19, no. 8, pp. 1366–1369, Aug. 2015.

[18] M. R. Bhatnagar and Arti M.K, "Performance analysis of hybrid satellite-terrestrial FSO cooperative system," *IEEE Photon. Technol. Lett.*, vol. 25, no. 22, pp. 2197–2200, Nov. 2013

[19] Q. Huang, M. Lin, W. Zhu, S. Chatzinotas, and M. Alouini, "Performance analysis of integrated satellite-terrestrial multiantenna relay networks with multiuser scheduling," *IEEE Trans. Aerosp. Electron. Syst.*, Early access, DoI: 10.1109/TAES.2019.2952698

[20] A. Viswanath, V. K. Jain, and S. Kar, "Analysis of earth-to-satellite free-space optical link performance in the presence of turbulence, beam-wander induced pointing error and weather conditions for different intensity modulation schemes, *IET Commun.*, vol. 9, no. 18, pp. 2253–2258, Dec. 2015.

[21] A. Viswanath, P. Gopal, V. K. Jain, and S. Kar, "Performance enhancement by aperture averaging in terrestrial and satellite free-space optical links, *IET Optoelectron.*, vol. 10, no. 3, pp. 111-117, May 2016.

[22] M. N. Pachery and M. R. Bhatnagar, "Double differential modulation for LEO-based land mobile satellite communication," *IEEE Trans. Aerosp. Electron. Syst.*, Early access, DoI: 10.1109/TAES.2020.2969543.

[23] M. Ju, H. K. Song, and I. M. Kim, "Joint relay-and-antenna selection in multi-antenna relay networks," *IEEE Trans. Commun.*, Vol. 58, No. 12, pp. 3417-3422, Dec. 2010.

[24] A. A. Farid and S. Hranilovic, "Outage capacity optimization for free space optical links with pointing errors," *J. Lightw. Technol.*, vol. 25, pp. 1702-1710, Jul. 2007

[25] L. Yang, J. Yuan, X. Liu, and M. O. Hasna, "On the performance of LAP-based multiple-hop RF/FSO systems," *IEEE Trans. Aerosp. Electron. Syst.*, vol. 55, no. 1, pp. 499-505, Feb. 2019.

[26] E. Zedini, A. Kammoun, and M. Alouini, "Performance of multibeam very high throughput satellite systems based on FSO feeder links with HPA nonlinearity," *IEEE Trans. Wireless Commun.*, Early access, DoI: 10.1109/TWC.2020.2998139.

[27] G. Pan, J. Ye, Y. Zhang, and M. Alouini, "Performance analysis and optimization of cooperative satellite-aerial-terrestrial systems," 2020, arXiv:2006.11854.

[28] H. Safi, A. Dargahi, J. Cheng, and M. Safari, "Analytical channel model and link design optimization for ground-to-HAP free-space optical communications," *J. Lightw. Technol.*, Early access, DoI: 10.1109/JLT.2020.2997806.

[29] M. Li, Y. Hong, C. Zeng, Y. Song and X. Zhang, "Investigation on the UAV-to-satellite optical communication systems," *IEEE J. Sel. Areas Commun.*, vol. 36, no. 9, pp. 2128-2138, Sept. 2018.

[30] R. Swaminathan, S. Sharma and A. S. MadhuKumar, "Performance analysis of HAPS-based relaying for hybrid FSO/RF downlink satellite communication," *in Proc. IEEE VTC Spring*, Antwerp, Belgium, 2020, pp. 1-5.

[31] C. Yan, L. Fu, J. Zhang and J. Wang, "A comprehensive survey on UAV communication channel modeling," *IEEE Access*, vol. 7, pp. 107769-107792, 2019.

[32] T. Pratt and J. Allnutt, *Satellite Communications* 3rd ed., John Wiley and Sons, Ltd., 2020.

[33] I. S. Ansari, F. Yilmaz, and M. Alouini, "Performance analysis of FSO links over unified Gamma-Gamma turbulence channels," *in Proc. IEEE VTC Spring*, Glasgow, 2015, pp. 1-5.

[34] The Wolfram Research Meijer G-function document. [Online]. Available: https://functions.wolfram.com/PDF/MeijerG.pdf

[35] M. K. Simon and M.-S. Alouini, *Digital Communications Over Fading Channels: A Unified Approach to Performance Analysis*, 2nd ed. New York, NY, USA: Wiley-Interscience, 2005.

[36] A. Abdi, W. C. Lau, M.-S. Alouini, and M. Kaveh, "A new simple model for land mobile satellite channels: first- and second-order statistics," *IEEE Trans. Wireless Commun.*, vol. 2, no. 3, pp. 519-528, May 2003.

[37] M. R. Bhatnagar and M. K. Arti, "On the closed-form performance analysis of maximal ratio combining in shadowed-Rician fading LMS channels," *IEEE Commun. Lett.*, vol. 18, no. 1, pp. 54–57, Jan. 2014.

[38] M. K. Arti, "Product of squared-SR random variables: application to satellite communication," *IEEE Trans. Aerosp. Electron. Syst.*, Early access, DoI: 10.1109/TAES.2019.2917488.

[39] I. S. Gradshteyn and I. M. Ryzhik, *Table of Integrals, Series, and Products*, 7th ed., Academic, 2007.

[40] H. Hemmati, ed., *Near-Earth Laser Communications*, CRC Press, 2009.

[41] G. Alfano and A. D. Maio, "Sum of squared shadowed-Rice random variables and its application to communication systems performance prediction," *IEEE Trans. Wireless Commun.*, vol. 6, no. 10, pp. 3540-3545, Oct. 2007.

[42] Swaminathan R, G. K. Karagiannidis, and R. Roy, "Joint antenna and relay selection strategies for decode-and-forward relay networks," *IEEE Trans. Veh. Technol.*, vol. 65, no. 11, pp. 9041–9056, Nov. 2016.

[43] E. W. Ng and M. Geller, "Table of integrals of the error functions," *Journal of Research of the National Bureau of Standards - B. Mathematical Sciences*, vol. 73B, no. 1, pp. 9041-9056, January-March 1969.

[44] "Examples of technical characteristics for unmanned aircraft control and non-payload communications links," ITU-R, Geneva, Tech. Rep. M.2233, 2012.